

## Supporting Information

# Unconventional Rate Law of Water Photooxidation at TiO<sub>2</sub> Electrodes

*Shufeng Zhang<sup>†\*</sup>, Wenhua Leng<sup>‡</sup>, and Kai Liu<sup>†\*</sup>*

<sup>†</sup> College of Engineering, Westlake University, Hangzhou, Zhejiang 310024, China

<sup>‡</sup> Department of Chemistry, Zhejiang University, Hangzhou, Zhejiang 310027, China

### Table of contents

<b>1</b>	<b>Comments on the rate law analysis in literatures</b> .....	3
<b>2</b>	<b>Theory background</b> .....	7
2.1	Rate constants derivation .....	8
2.2	Surface hole density derivation.....	11
<b>3</b>	<b>Photoanode preparation</b> .....	13
<b>4</b>	<b>Material Characterizations</b> .....	13
<b>5</b>	<b>(Photo-)electrochemical experiments and results</b> .....	17

---

\*Corresponding Author. E-mail: [Alisen9117@163.com](mailto:Alisen9117@163.com); [liukai@westlake.edu.cn](mailto:liukai@westlake.edu.cn).

5.1	Photoelectrochemical performance.....	19
5.2	Electrochemical impedance spectroscopy (EIS) results .....	21
5.3	Derivation of $k_{ct}$ .....	28
5.4	Derivation of $k_{sr}$ .....	30
5.5	Fitted results of potential dependent rate constants .....	32
5.6	Verification of $k_{ct}$ and $k_{sr}$ .....	34
5.7	Mott-Schottky measurements .....	34
5.8	Cyclic voltammetry (CV) measurements.....	37
5.9	Bandgap states measurements.....	38
5.10	$I$ - $V$ curves at the presence of hole scavengers .....	43
5.11	Comparison of measured and calculated photocurrent.....	45
5.12	Relationship of $k_{ct}$ and $k_{sr}$ with surface hole density <b><math>pss_0</math></b> .....	46
<b>6</b>	<b>Comparison with relevant work</b> .....	<b>49</b>
<b>7</b>	<b>Implication on kinetic study</b> .....	<b>52</b>
<b>8</b>	<b>Reference</b> .....	<b>53</b>

## 1 Comments on the rate law analysis in literatures

In chemistry, to establish a rate equation, it is generally necessary to obtain all kinetic parameters and correlate them with the reaction rate. For water photooxidation on n-type semiconductor, at least three parameters/variables are required in order to calculate the reaction rate (in terms of photocurrent), as expressed in **eq. S1** where  $j_{st}$  is the steady state photocurrent,  $k_{ct}$  is the apparent charge transfer rate constant,  $[h_s^+]$  is the surface hole density,  $n$  is the rate order with respect to hole density.

$$j_{st} = k_{ct}[h_s^+]^n \quad (\text{S1})$$

Any appropriate rate law should at least satisfy that the calculated rates (by the right hand of **eq. S1**) equal the measured (by left hand of **eq. S1**). Ideally, it may be the best if the three parameters in the right hand of **eq. S1** are obtained not relying on the measured rate (left hand of **eq. S1**). This allows us to employ the measured  $j_{st}$  as a diagnostic criterion for the validity of rate law. If the measured  $j_{st}$  is used to simultaneously obtain both  $k_{ct}$  and  $n$  through fitting with known  $[h_s^+]$ , then one needs other independent evidence to justify any of  $k_{ct}$  and  $n$ , because one admits in advance that the rate equation is always correct.

Several studies<sup>1-5</sup> have attempted to derive the partial kinetic parameters from rate law analysis of **eq. S1**. The value of  $n$  is obtained in the literatures<sup>1-5</sup> by this fitting approach with the assumption that  $k_{ct}$  is constant. But the assumption is not justified at all or independently. On the contrary, other researchers and we have demonstrated that the assumption is invalid and  $k_{ct}$  is light intensity/surface hole density dependent<sup>6-8</sup>. As shown in **Figure S1 a**, the  $j_{st}$  vs.  $[h_s^+]$  data reported in the previous report<sup>1</sup> for TiO<sub>2</sub>

can be well described by a rate law with surface hole density dependence of apparent rate constant, as described by **eq. (17)**. More evidences that support the reported rate law is incorrect can be found in the main text and below. For instance, the reported rate law could not explain the nonlinear relationship between  $[h_s^+]$  and light intensity/photocurrent, and pH dependence of photocurrent. We argue that any of these three points is enough to question the reported rate law. Otherwise, if their rate equation proposed in the previous reports<sup>1</sup> is appropriate, then the  $k_{ct}$  calculated from this rate equation as described in **eq. S2**, should be a constant and independent of  $[h_s^+]$ .

$$k_{ct} = \frac{j_{st}}{[h_s^+]^n} \quad (\text{S2})$$

According to their experimental results<sup>1</sup>, the  $\ln k_{ct}$  is almost a constant under the acidic and neutral conditions. However, a  $[h_s^+]$  dependence of  $\ln k_{ct}$  is observed in pH 13.6 as shown in **Figure S1 b-d**, which contradicts to their rate equation.

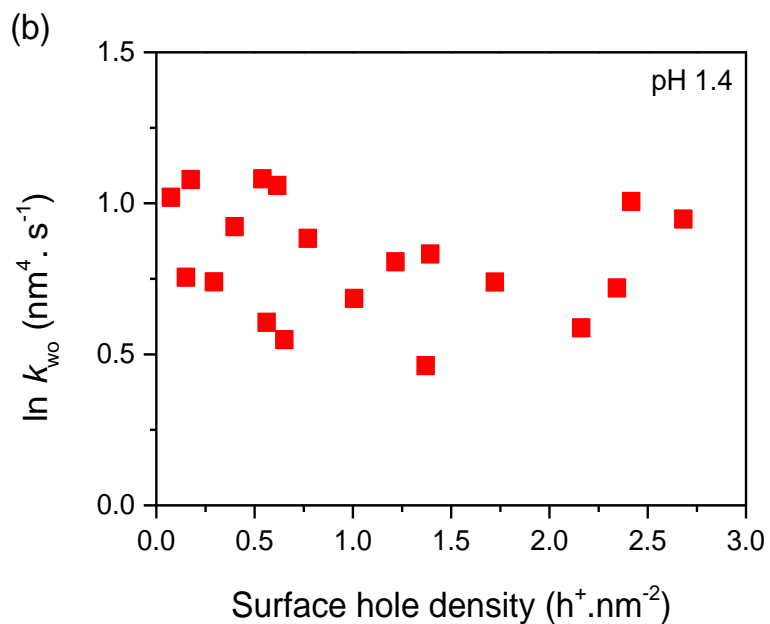
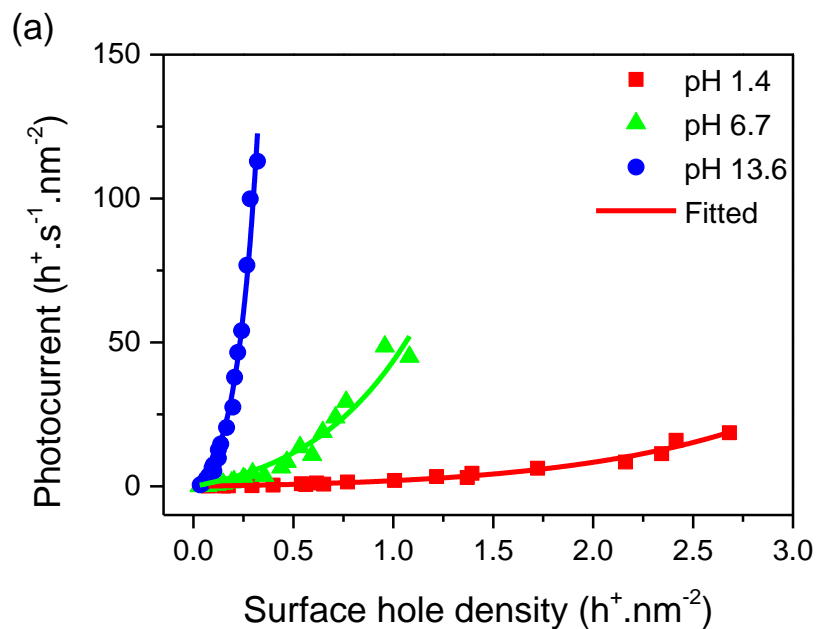
Similarly, according to their rate equation<sup>1</sup>,  $[h_s^+]$  is expected to be *always* proportional to  $\sqrt[n]{j_{st}}$  since the  $k_{ct}$  is supposed to be constant as given by **eq. S3**:

$$[h_s^+] = \sqrt[n]{\frac{j_{st}}{k_{ct}}} \quad (\text{S3})$$

But, as we stated in the main text, this fails to explain their experimental results shown in Figure S17 in the previous report<sup>1</sup>: with the increasing light intensity ( $\Phi_0$ , ~0.001 to 1 sun),  $j_{st}$  is *always* increased linearly (the black hollow dot;  $j_{st} \propto \Phi_0$ ) while  $[h_s^+]$  (the blue solid square point) is gradually saturated at high light intensity. This is also contradictory to their rate equation.

Besides, according to their proposed rate equation<sup>1</sup>, the photocurrent should be irrelevant to pH since the  $k_{ct}$  is constant (independent on pH). However, it is well-

documented that the photoelectrochemical performance of TiO<sub>2</sub> water oxidation is pH dependent.<sup>9-13</sup> Thus, their proposed rate law is questionable.



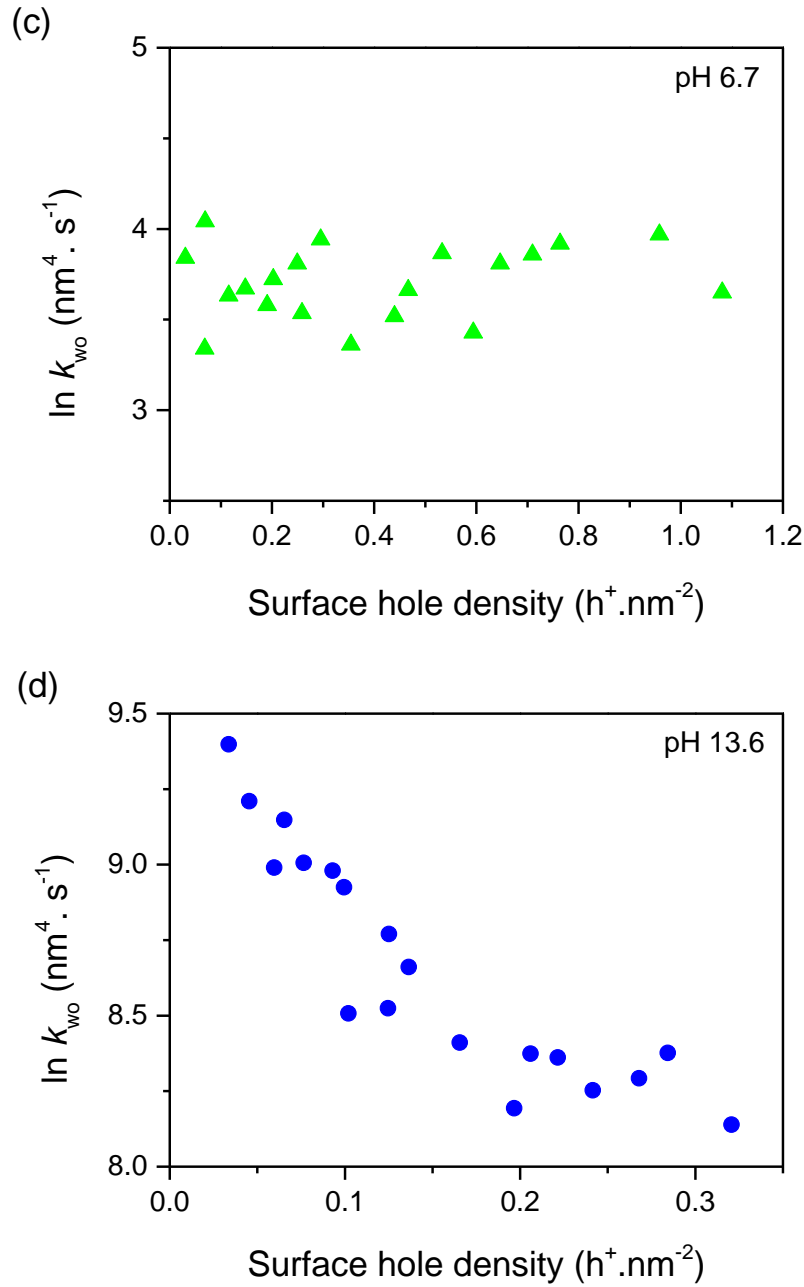


**Figure S1.** (a) Relationship between density of accumulated surface holes and photocurrent and fitted by our rate equation of **eq. (17)**; relationship between  $\ln k_{ct}$  and density of surface holes  $[h_s^+]$  for  $TiO_2$  electrodes at various pHs: (b) pH 1.4; (c) pH 6.7; pH 13.6. Data were from **Figure 6** (the same as **Figure. S21**) in the reference paper<sup>1</sup> (which can be obtained from <http://zenodo.org> with the identifier 10.5281/zenodo.851635 in **Ref 14**<sup>14</sup>) and they were just shown in linear-linear scale

here while they are plotted in logarithm of both X and Y axis (log-log plot) in the previous work<sup>1</sup>.

## 2 Theory background

As mentioned in the manuscript, in our model, the applied potential ( $\varphi$ ) which drops across the semiconductor liquid junction (SCLJ) is regarded to be distributed between the part of space charge layer ( $\varphi_{SC}$ ) and that of Helmholtz layer ( $\varphi_H$ ). For bulk photoanode, a capacitance of the space charge layer ( $C_{SC}$ ) is normally existed in the semiconductor side of the interface, which can be generally described by Mott-Schottky relation. The capacitance of Helmholtz layer ( $C_H$ ) at the electrolyte side of the interface is normally assumed to be a constant.

The  $\varphi_{SC}$  dropped on space charge layer changes surface density of electrons ( $n_s$ ), which approximately follows the Boltzmann distribution. Since the surface recombination rate is linearly dependent on  $n_s$ , the apparent surface recombination rate constant  $k_{sr}$  can be described by **eq. S4**, where  $k_{sr}^0$  is the value of  $k_{sr}$  at  $\varphi_{SC}=0$ ,  $\alpha$  is the ideality factor,  $q$  is the elementary charge,  $k_B$  is the Boltzmann constant, and  $T$  is the temperature.

$$k_{sr} = k'_{sr} n_s = k_{sr}^0 \exp\left(\frac{-\alpha q \varphi_{SC}}{k_B T}\right) \quad (\text{S4})$$

The  $\varphi_H$  is assumed to affect the apparent charge transfer rate constant  $k_{ct}$  by altering the activation energy, thus, the Tafel equation can be used to describe the potential dependence of  $k_{ct}$  as given in **eq. S5**, where  $k_{ct}^0$  is the value of  $k_{ct}$  at  $\varphi_H = 0$  and is related the density of the electron donor [ $D$ ],  $\beta$  is the charge transfer coefficient and

normally regarded to be 0.5.

$$k_{ct} = k_{ct}^0 \exp\left(\frac{\beta q \phi_H}{\kappa_B T}\right) \quad (\text{S5})$$

For simplicity, the rate constant  $k_{\text{trap}}$ , which represents the process of hole captured by surface state, is assumed to be independent to potential drop in the depletion layer.<sup>15</sup>

The time-dependent surface hole density can be described by convention kinetic differential equations (or continuity equation) as reported previously<sup>15, 16</sup>. The differential equations for the holes at the valence band and surface state is given by **eq. S6** and **S7**, respectively, where  $p_{\text{VB}}$  is the charge density associated with free holes at the surface,  $p_{\text{ss}}$  is the charge density for holes captured in surface states.

$$\frac{dp_{\text{VB}}}{dt} = I_0 - k_{\text{VB}} p_{\text{VB}} \quad (\text{S6})$$

$$\frac{dp_{\text{ss}}}{dt} = k_{\text{trap}} p_{\text{VB}} - k_{\text{ct}} p_{\text{ss}} - k_{\text{sr}} p_{\text{ss}} \quad (\text{S7})$$

Under steady-state conditions where  $\frac{dp_{\text{VB}}}{dt} = 0$  and  $\frac{dp_{\text{ss}}}{dt} = 0$ , thus according to **eqs. S6** and **S7**, the steady state concentration of photohole accumulated in the surface state,  $p_{\text{ss}}^0$ , can be written as **eq. S8**.

$$p_{\text{ss}}^0 = \frac{I_0}{(k_{\text{ct}} + k_{\text{sr}})} \quad (\text{S8})$$

In this case, according to **eq. S7**, the steady state photocurrent,  $j_{\text{st}}$ , is described by  $j_{\text{st}} = k_{\text{ct}} p_{\text{ss}}^0$ . Inserting **eq. S8** into this equation, we get:

$$j_{\text{st}} = k_{\text{ct}} p_{\text{ss}}^0 = \frac{k_{\text{ct}} I_0}{(k_{\text{ct}} + k_{\text{sr}})} \quad (\text{S9})$$

## 2.1 Rate constants derivation

The electrochemical impedance spectroscopy (EIS) is well recognized as a powerful tool to obtain rate constants,<sup>8, 15, 17, 18</sup> thus is employed in the current study.

During EIS experiment, the illumination intensity remains unchanged. So the flux of

hole ( $I_0$ ) can be approximately considered as a constant if the penetration depth of the light is smaller than the width of the depletion layer.<sup>19</sup> Besides, a small sinusoidal signal potential perturbation ( $\tilde{U}$ ) with the frequency  $\omega/2\pi$  is applied across the photoelectrochemical cell. If electrolyte resistance ( $R_s$ ) is compensated or is sufficiently small, then  $\tilde{U}$  can be described by **eq. S10**.

$$\tilde{U} \approx \tilde{\varphi} = \tilde{\varphi}_{sc} + \tilde{\varphi}_H \quad (\text{S10})$$

Perturbation  $\tilde{U}$  will lead to change in  $\tilde{\varphi}_{sc}$  and  $\tilde{\varphi}_H$ . The variation of  $\tilde{\varphi}_{sc}$  should result in charging and discharging of the surface state capacitance ( $C_{SS}$ ) and the  $C_{SC}$ . While the variation of  $\tilde{\varphi}_H$  will lead to charging and discharging of the Helmholtz layer. The resulting current density ( $\tilde{j}$ ) variation can be given by **eq. S11**<sup>15</sup>, where  $\tilde{j}^{SC}$  is the faradic component in semiconductor side,  $\tilde{j}^{SS}$  is current due to charging of the surface state capacitance,  $\tilde{j}^H$  is the faradic component in electrolyte side,  $\omega$  is the angular frequency and  $i = \sqrt{-1}$

$$\tilde{j} = \tilde{j}^{SC} + (i\omega C_{SC}\tilde{\varphi}_{sc} + \tilde{j}^{SS}) = \tilde{j}^H + i\omega C_H\tilde{\varphi}_H \quad (\text{S11})$$

The electrochemical impedance  $Z(\omega)$  is the inverse of the electrochemical admittance  $Y(\omega)$  that is defined as the ratio of  $\tilde{j}/\tilde{U}$ . The theoretic impedance expression can be derived with **eqs. S4 to S11**, which is given by **eq. S12**<sup>15</sup> (see detailed derivation of  $Z(\omega)$  in the Appendix of the previous report<sup>15</sup>).

$$Z(\omega) = R_s + \frac{C_H + C_{SC} + \frac{C_{SS}}{1+i\omega\tau_{SS}} + \frac{\alpha\left(\frac{q}{\kappa_B T}\right)k_{sr}I_0 + \beta\left(\frac{q}{\kappa_B T}\right)k_{ct}I_0}{(k_{ct}+k_{sr})(k_{ct}+k_{sr}+i\omega)}}{C_H \left[ i\omega \left( C_{SC} + \frac{C_{SS}}{1+i\omega\tau_{SS}} \right) + \frac{\alpha\left(\frac{q}{\kappa_B T}\right)k_{sr}I_0(k_{ct}+i\omega)}{(k_{ct}+k_{sr})(k_{ct}+k_{sr}+i\omega)} \right] + \left( C_{SC} + \frac{C_{SS}}{1+i\omega\tau_{SS}} \right) \frac{\beta\left(\frac{q}{\kappa_B T}\right)k_{ct}I_0(k_{sr}+i\omega)}{(k_{ct}+k_{sr})(k_{ct}+k_{sr}+i\omega)} + \frac{\alpha\left(\frac{q}{\kappa_B T}\right)k_{sr}I_0\beta\left(\frac{q}{\kappa_B T}\right)k_{ct}I_0}{(k_{ct}+k_{sr})^2(k_{ct}+k_{sr}+i\omega)}}} \quad (\text{S12})$$

where  $\tau_{SS}$  is the time constant of charging of surface state.

According to previous reports,<sup>8, 15, 20</sup> the arc of the second semicircle on the

Nynquist plot ( $Z_{\text{sec}}(\omega)$ ) is associated with charge transfer and surface recombination process. The mathematic equation for the theoretical impedance at low frequency can be described by **eq.S13**<sup>15</sup> (see detailed derivation of  $Z_{\text{sec}}(\omega)$  in the Appendix of the previous report<sup>15</sup>).

$$Z_{\text{sec}}(\omega) = \frac{1 + \frac{\alpha\left(\frac{q}{\kappa_{\text{B}}T}\right)k_{\text{sr}}I_0 + \beta\left(\frac{q}{\kappa_{\text{B}}T}\right)k_{\text{ct}}I_0}{(C_{\text{H}}+C_{\text{SC}})(k_{\text{ct}}+k_{\text{sr}})(k_{\text{ct}}+k_{\text{sr}}+i\omega)}}{\frac{\alpha\left(\frac{q}{\kappa_{\text{B}}T}\right)k_{\text{ct}}k_{\text{sr}}I_0}{(C_{\text{H}}+C_{\text{SC}})(k_{\text{ct}}+k_{\text{sr}})(k_{\text{ct}}+k_{\text{sr}}+i\omega)} \left( C_{\text{H}}+C_{\text{SC}} + \frac{\beta\left(\frac{q}{\kappa_{\text{B}}T}\right)I_0}{k_{\text{ct}}+k_{\text{sr}}} \right) + \frac{i\omega \left[ \alpha\left(\frac{q}{\kappa_{\text{B}}T}\right)C_{\text{H}}k_{\text{sr}}I_0 + \beta\left(\frac{q}{\kappa_{\text{B}}T}\right)C_{\text{SC}}k_{\text{ct}}I_0 \right]}{(C_{\text{H}}+C_{\text{SC}})(k_{\text{ct}}+k_{\text{sr}})(k_{\text{ct}}+k_{\text{sr}}+i\omega)}}} \quad (\text{S13})$$

The angular frequency of the maximum imaginary component of the second arc ( $\omega_{\text{max}}^1$ ), which is the time constant of charge transfer process, is equal to the apparent charge transfer rate constant  $k_{\text{ct}}$ . The  $\omega_{\text{max}}^1$  can be obtained by the theoretic analysis of **eq. S13**, which can be expressed as **eq. S14**.<sup>15</sup>

$$\omega_{\text{max}}^1 = k_{\text{ct}}^0 \left[ 1 + \frac{C_{\text{SC}}}{C_{\text{H}}} + \frac{\beta q I_0}{\kappa_{\text{B}} T C_{\text{H}} (k_{\text{ct}} + k_{\text{sr}})} \right] = k_{\text{ct}}^0 \left( 1 + \frac{C_{\text{SC}}}{C_{\text{H}}} \right) + \frac{j_{\text{st}} \beta q}{\kappa_{\text{B}} T C_{\text{H}}} \quad (\text{S14})$$

According to **eq. S14**, the  $\omega_{\text{max}}^1$  is affected by 3 parts: **1)** the first part is caused by the potential drop on the space charge layer  $\varphi_{\text{SC}}$ ; **2)** the potential drop across the Helmholtz layer  $\varphi_{\text{H}}$ ; **3)** the accumulation of photoholes on the surface states. Therefore, as long as  $\frac{C_{\text{SC}}}{C_{\text{H}}} + \frac{\beta q p_{\text{SS}}^0}{\kappa_{\text{B}} T C_{\text{H}}} \ll 1$  is not satisfied, the  $k_{\text{ct}}$  is expected to be potential and light intensity dependent. On the other hand, if the applied potential drops only on the space charge layer (for the case  $C_{\text{SC}} \ll C_{\text{H}}$ ) and the effect of the photohole accumulation can be completely ignored (for the case  $I_0 \ll C_{\text{H}}(k_{\text{ct}} + k_{\text{sr}})\kappa_{\text{B}}T/\beta q$ ), then  $k_{\text{ct}}$  is considered as a constant and is independent of potential and light intensity, as described in **eq.S15**.<sup>15</sup> This is the model adopted for the rate law analysis of water photo-oxidation on  $\text{TiO}_2$  in **Ref 1**.<sup>1</sup>

$$\omega_{\text{max}}^1 = k_{\text{ct}} \quad (\text{S15})$$

Besides, under high light intensity (for the case  $I_0 \gg C_H(k_{ct} + k_{sr})\kappa_B T/\beta q$ ), the  $\omega_{max}^1$  is expected to be proportional to  $j_{st}$  as in this case the **eq. S14** can be expressed as **eq.S16**.<sup>15</sup>

$$\omega_{max}^1 = \frac{\beta q k_{ct} I_0}{\kappa_B T C_H (k_{ct} + k_{sr})} = \frac{\beta q}{\kappa_B T C_H} j_{st} \quad (\text{S16})$$

Furthermore, the  $k_{sr}$  can be obtained either by mathematic fitting of the **eq. S13**, or from the ratio of **eq. 37** and **41** from **Ref 15**<sup>15</sup> when the incident light intensity is weak, and  $k_{ct}$  is known. The  $C_{SC}$  can be estimated by Mott-Schottky measurement and  $C_H$  can be obtained from the slope of  $\omega_{max}^1$  vs.  $j_{st}$  (**eq. S16**). This ratio is presented in **eq. S17** where  $Z_{\omega \rightarrow 0}$  represents the lowest frequency point and  $Z_{high}$  is the intersect point of the real axis of the second semicircle arc in the Nynquist plots.<sup>15</sup>

$$\frac{Z_{\omega \rightarrow 0}}{Z_{high}} = \frac{(k_{ct} + k_{sr})^2 / \left[ \alpha \left( \frac{q}{\kappa_B T} \right) k_{ct} k_{sr} I_0 \right]}{(C_H + C_{SC})(k_{ct} + k_{sr})\kappa_B T / \alpha q C_H k_{sr} I_0} = \frac{C_H (k_{ct} + k_{sr})}{k_{ct} (C_H + C_{SC})} \quad (\text{S17})$$

## 2.2 Surface hole density derivation

The characteristics of the interface states can also be investigated by the impedance response as reported previously.<sup>15, 21-24</sup> The impedance due to filling and emptying of the interface states give rise to an additional response ( $Z_{SS}$ ). Measured  $Z_{SS}$  consists electrolyte resistance ( $R_S$ ) and a serial pseudo-capacitance ( $C_p(\omega)$ ), which is the response of interface states. The total measured capacitance is simply the sum of  $C_p(\omega)$  and  $C_{SC}$ , which can be obtained from real  $Re(Z)$  and imaginary  $Im(Z)$  parts of the measured impedance, as shown in **eq.S18** and **S19**.<sup>21, 22</sup>

$$C_p(\omega) = [\omega Im(Z)(1 + D^2)]^{-1} - C_{sc} \quad (\text{S18})$$

$$D = \left[ \frac{Re(Z) - R_S}{-Im(Z)} \right] \quad (\text{S19})$$

According to previous report<sup>22</sup>, if interface states interact with the conduction band electron under illumination, which means they function as recombination center. The density of the occupied states ( $S_{\text{tot}}^-$ ) is given by **eq.S20** and the  $C_p(\omega)$  is described by **eq.S21** where  $S_{\text{tot}}$  is the density of the surface state<sup>22</sup>.

$$S_{\text{tot}}^- = \frac{k_{\text{sr}}}{(k_{\text{trap}} + k_{\text{sr}})} S_{\text{tot}} \quad (\text{S20})$$

$$C_p(\omega) = \frac{q^2}{k_{\text{B}}T} \frac{(k_{\text{sr}})^2 k_{\text{trap}}}{(k_{\text{sr}} + k_{\text{trap}})} \frac{S_{\text{tot}}}{\omega^2 + (k_{\text{sr}} + k_{\text{trap}})^2} \quad (\text{S21})$$

When plotting  $C_p(\omega)$  vs. applied potential (implicit in  $k_{\text{sr}}$ ) for various frequency by **eq. (21)**, we can easily find that the  $C_p(\omega)$  has a frequency-dependent maximum approximately at the potential, where (derived with the help of  $dc_p(\omega)/d\phi = dc_p(\omega)/dk_{\text{sr}} * dk_{\text{sr}}/d\phi = 0$ , and  $dk_{\text{sr}}/d\phi = -k_{\text{sr}}^0 \alpha q k_{\text{sr}} / k_{\text{B}}T$  according to **eq. 1**)

$$k_{\text{sr}} = k_{\text{trap}} + \sqrt{(k_{\text{trap}})^2 + \omega^2} \quad (\text{S22})$$

For the low frequency limit ( $\omega \rightarrow 0$ ), **eq. S22** can be approximated to be:

$$k_{\text{sr}} = 2k_{\text{trap}} \quad (\text{S23})$$

By substituting **eq. S23** into **eq. S20** and **S21** respectively, we will get:

$$S_{\text{tot}}^- = \frac{2}{3} S_{\text{tot}} \quad (\text{S24})$$

$$C_p(\text{max})_{\omega \rightarrow 0} = \frac{4q^2}{27k_{\text{B}}T} S_{\text{tot}} \quad (\text{S25})$$

Where  $C_p(\text{max})_{\omega \rightarrow 0}$  is the maximum capacitance at the low frequency limit.

From **eq. S25**, the density of the recombination centers,  $S_{\text{tot}}$ , can be obtained from the measured  $C_p(\text{max})_{\omega \rightarrow 0}$ . Once  $S_{\text{tot}}$  at the low frequency is known, the density of the unoccupied surface state ( $S_{\text{tot}}^0$ ) can be obtained ( $S_{\text{tot}}^0 = S_{\text{tot}} - S_{\text{tot}}^- = \frac{1}{3} S_{\text{tot}}$ ), which is assumed to be the value of  $p_{\text{SS}}^0$ .

### **3 Photoanode preparation**

The TiO<sub>2</sub> photoanode was prepared on fluorine-doped tin oxide conducting glass (FTO, 2.2 mm thick, 7 Ω/square, Wuhan Jingge Co., Ltd, China) using a slightly modified sol-gel method.<sup>25,26</sup> Briefly, the precursor solution was prepared by dissolving titanium butoxide (34 mL, 99%, Sigma Aldrich) in ethanol (11.7 mL) with hydrolysis control agent solution, which contains a mixture of Milli-Q water (0.4 mL, Millipore Corp., 18.2 MΩ cm at 25 °C), HCl (2.0 mL), and ethanol (11.7 mL). The precursor solution was spin-coated onto the FTO glass. The coated glass was dried at the room temperature and subsequently heated inside a muffle furnace (Nabertherm, N7/H, Germany) in air at 500 °C for 10 min before cooled to room temperature. This procedure was repeated 8 times, and then the film was annealed in air at 500 °C for 1 h.

### **4 Material Characterizations**

The morphology and elemental analysis of the photoanode were examined by scanning electron microscope (SEM, Zeiss Gemini 500, Carl Zeiss, UK) at an accelerating voltage of 5 kV. Elemental analysis was done with the equipped energy dispersive X-ray spectrometer (EDS, Oxford Instrument, Oxford, UK). X-ray photoelectron spectroscopy (XPS) was carried out to investigate the chemical composition of the photoanode, using a Thermo Fisher ESCALAB Xi+ spectrometer with monochromatic Al Kα radiation. Survey scan was collected over the 0~1486 eV binding energy range with 1 eV resolution and a pass energy of 100 eV while the

elemental scans were collected with 0.1 eV resolution and a pass energy of 30 eV. Peak positions were calibrated to the C1s level (284.80 eV) due to surface contaminants. The phase of the TiO<sub>2</sub> photoanode was identified using X-ray diffraction (XRD), which were measured with a Bruker D8 Advance diffractometer equipped with Cu source and energy resolved LynxEye XE-T detector. The XRD of the patterns were collected between  $10^{\circ} \leq 2\theta \leq 70^{\circ}$  with a step size of 0.0172°.

It is observed that relatively flat and uniform layer was grown on FTO surface (**Figure S2 a**). The thickness is about 9.2 μm according to cross section image (**Figure S2 b**), consistent with profilometer measurement (Bruker DektakXT). The EDS results show the existence of Ti and O element and no other elements were observed (**Figure S3**). XPS survey spectrum of the photoanode is presented in **Figure S4 a** with the appearance of Ti and O element, consistent with EDS results. Typical high-resolution spectrum of Ti2p is shown in **Figure S4 b**, peaks located at 458.9 and 464.4 eV can be attributed to the characteristic spin-orbit split 2p<sub>3/2</sub> and 2p<sub>1/2</sub>, respectively. This suggests that the valence of titanium on the surface is mainly +4, supported by other literatures.<sup>27,</sup>  
<sup>28</sup> The peak situated at 530.1~532.2 eV (**Figure S4 c**) can be assigned to O1s. According to previous reports,<sup>27,28</sup> the binding energy at 530.1 eV can be assigned to lattice oxygen while the shoulder peak at 532.2 eV may be resulted from the absorbed oxygen species in the samples. As shown in **Figure S5**, the TiO<sub>2</sub> photoanode exhibits a series of characteristic diffraction peaks that can be well indexed to the anatase TiO<sub>2</sub> (PDF#03-065-5714), except two additional peaks that are attributed to the response of SnO<sub>2</sub> (PDF#41-1445) from FTO substrate. To sum up, these results clearly indicate that the

photoanode studied herein is bulk TiO<sub>2</sub> in anatase phase.

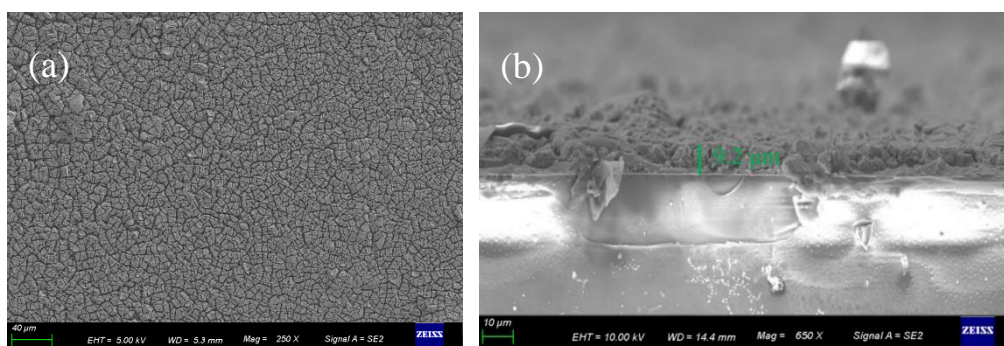


**Figure S2.** a) Typical top-view SEM image. b) cross section image.

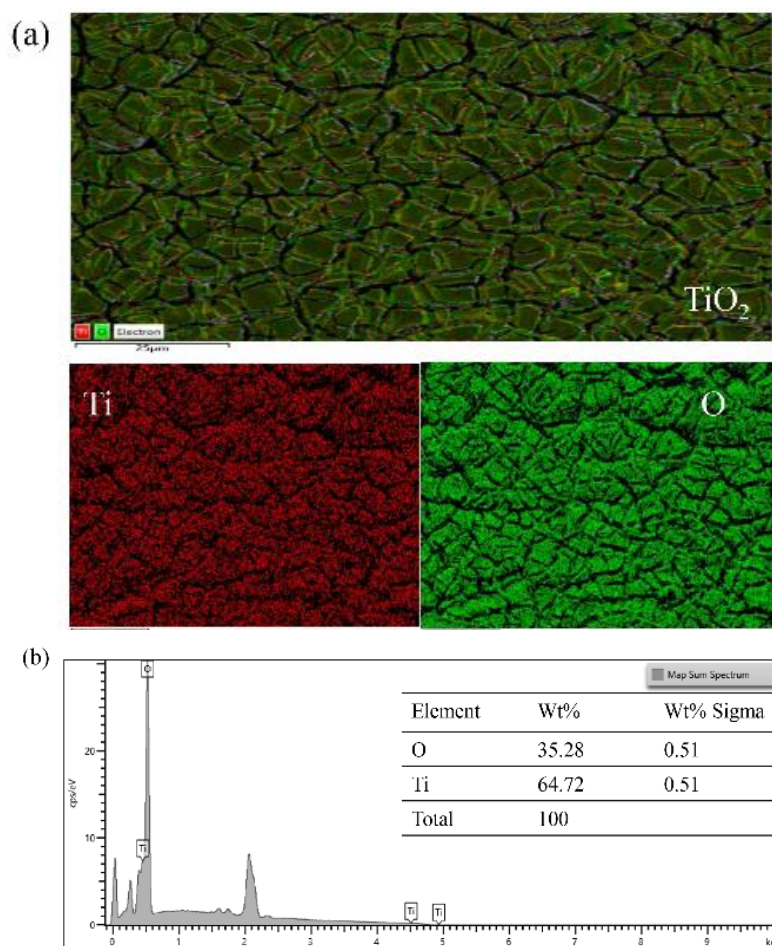


**Figure S3.** a) EDS mapping and b) EDS spectra of the photoanode.

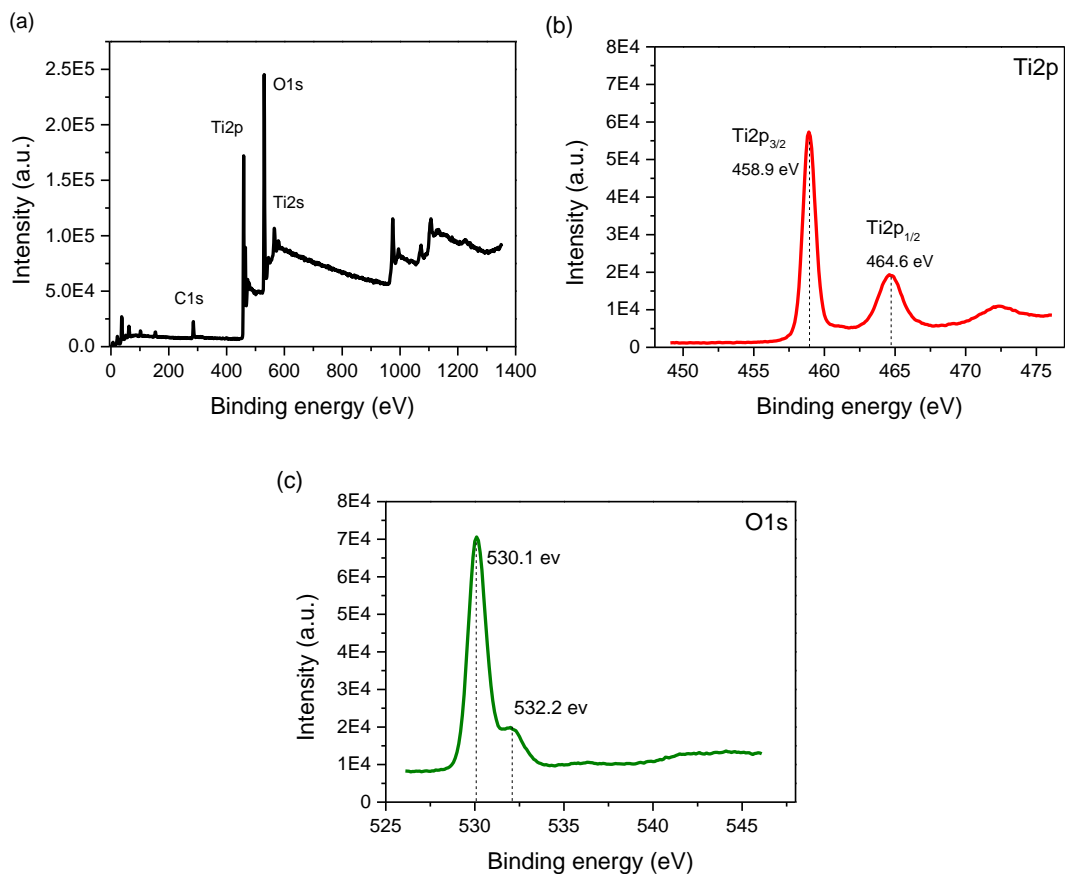


**Figure S4.** a) XPS full spectrum. b) high resolution XPS of Ti2p. c) high resolution XPS of O1s.

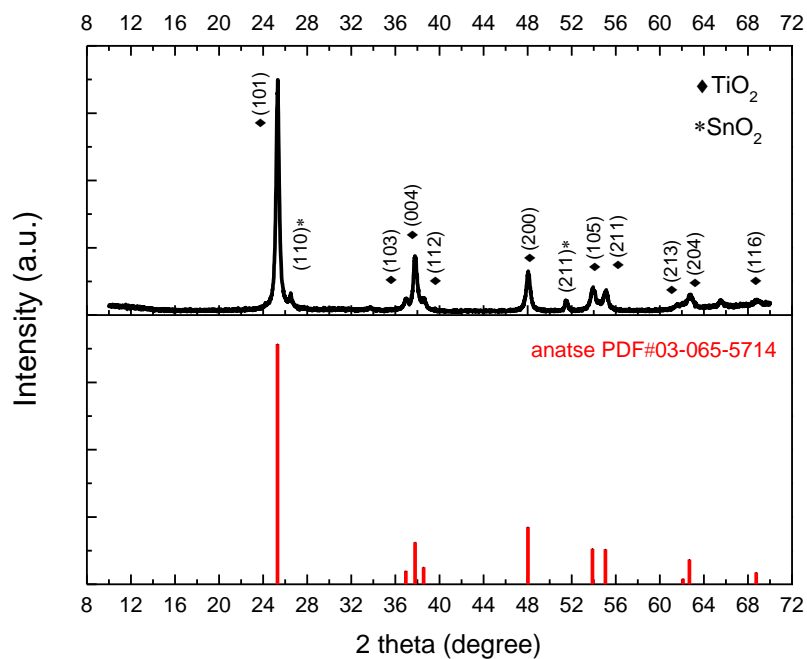


**Figure S5.** XRD pattern result.

## 5 (Photo-)electrochemical experiments and results

The (photo-)electrochemical experiments were performed in a conventional three-electrode cell. The film electrode was used as a working electrode, a large surface area of Pt mesh as a counter electrode and all potentials were measured against a calomel reference electrode (SCE). The electrolyte was aqueous solution of different pH: 0.5 M NaClO<sub>4</sub> at pH 2.0 (pH adjusted by HClO<sub>4</sub>), and 0.1 M NaClO<sub>4</sub> with 0.1 M Na<sub>2</sub>HPO<sub>4</sub> and 0.1 M NaH<sub>2</sub>PO<sub>4</sub> at pH 6.6, and 0.5 M NaOH at pH 13.4. In view of the fact that oxygen reduction could take place on TiO<sub>2</sub> photoanode,<sup>29</sup> all electrolyte were purged with nitrogen prior experiment to remove O<sub>2</sub>. The evidence of the complete removal of O<sub>2</sub> for the photoelectrochemical experiments was presented in **Figure S6**.

The electrochemical station (Reference 600, Gamry Co. Ltd., USA) was used as constant voltage source. For illuminated experiments, the light source was a 150 W xenon lamp (Newport 6255) coupled with an AM 1.5 global filter (Newport 81094) and was incident from the electrolyte-electrode side. The light intensity was measured by a photodiode (S370, UDT instrument). The illuminated surface area of the photoelectrodes was 0.5 cm<sup>2</sup> (0.8 cm in diameter).

For (photo)electrochemical impedance spectroscopy (EIS), the frequency range was from 100 kHz to 0.01 Hz, using a 10 mV sinusoidal potential modulation. The Mott-Schottky experiments were performed at 10 kHz by applying the starting potential for 1 min and then performing a potential scan from negative to positive with a potential step of 50 mV. Other experimental conditions were identical as those for the EIS measurements. Impedance measurements for analysis of interface states and

recombination centers were the similar to the Mott-Schottky experiments, with a 5 mV (rms) amplitude at changing frequencies.

All experiments were performed at room temperature, and comparative experiments were performed over an identical photoanode. If needed, the data presented in this work was generally with respect to the apparent surface area of the photoanode. Although there may be deviation compared the electroactive area of the photoanode, it may not affect the comparison results, which is the main scope of this manuscript.

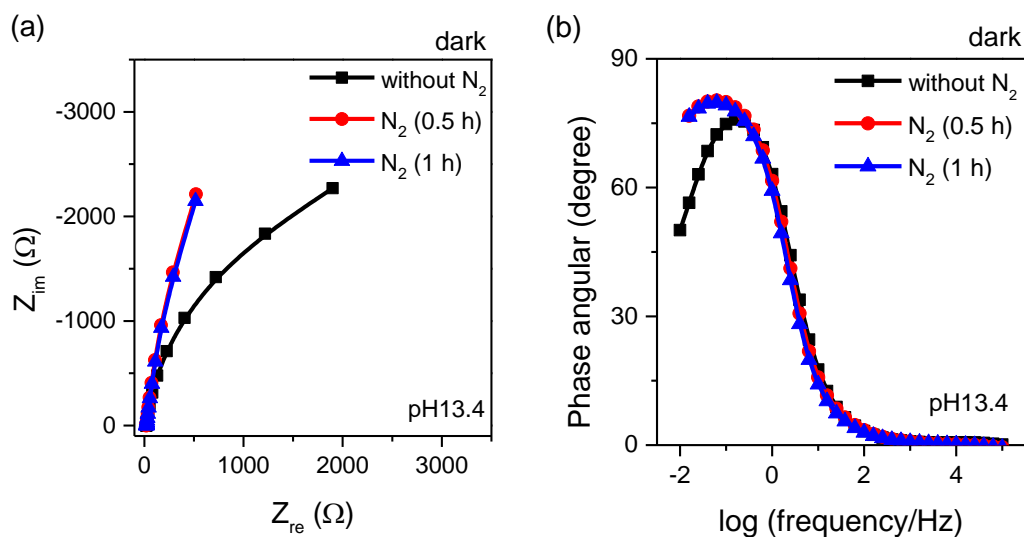
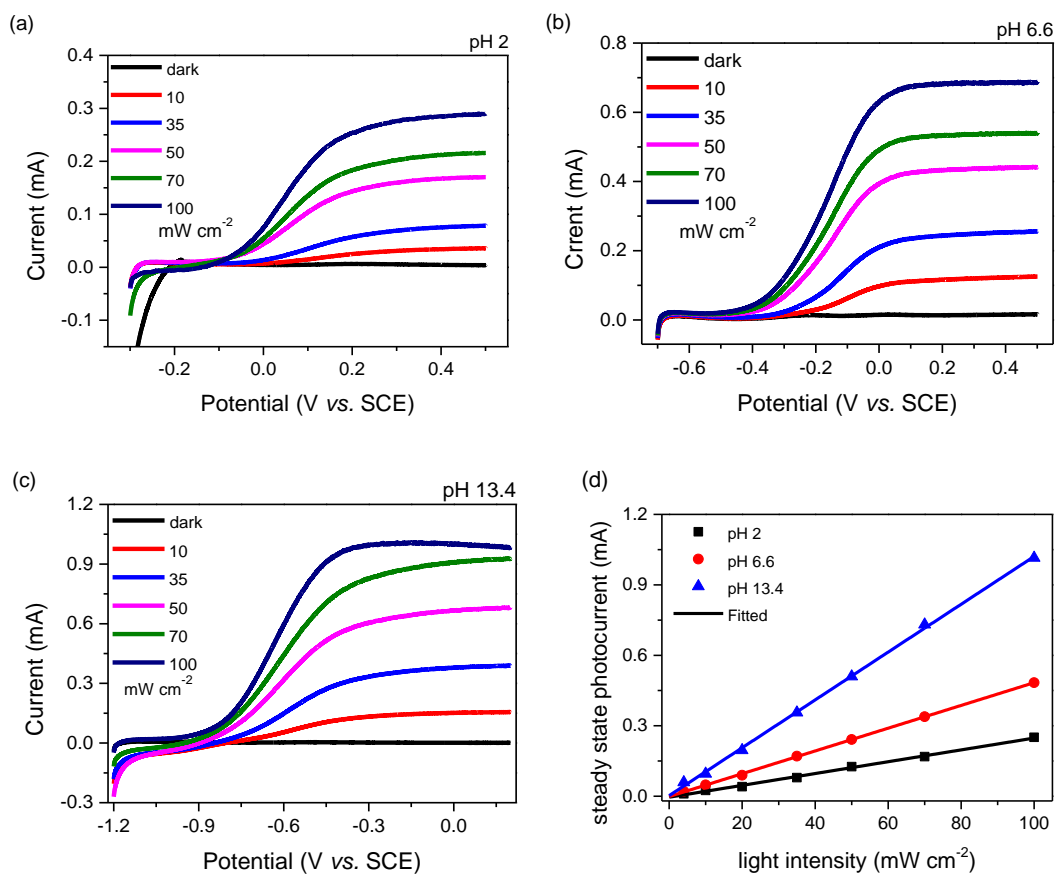


**Figure S6.** The EIS responses of TiO<sub>2</sub> photoanode at the open circuit potential in the dark at electrolyte of pH 13.4 before and after N<sub>2</sub> was purged for different time: **a)**

Nynquist plot. **b)** Bode plot.

## 5.1 Photoelectrochemical performance

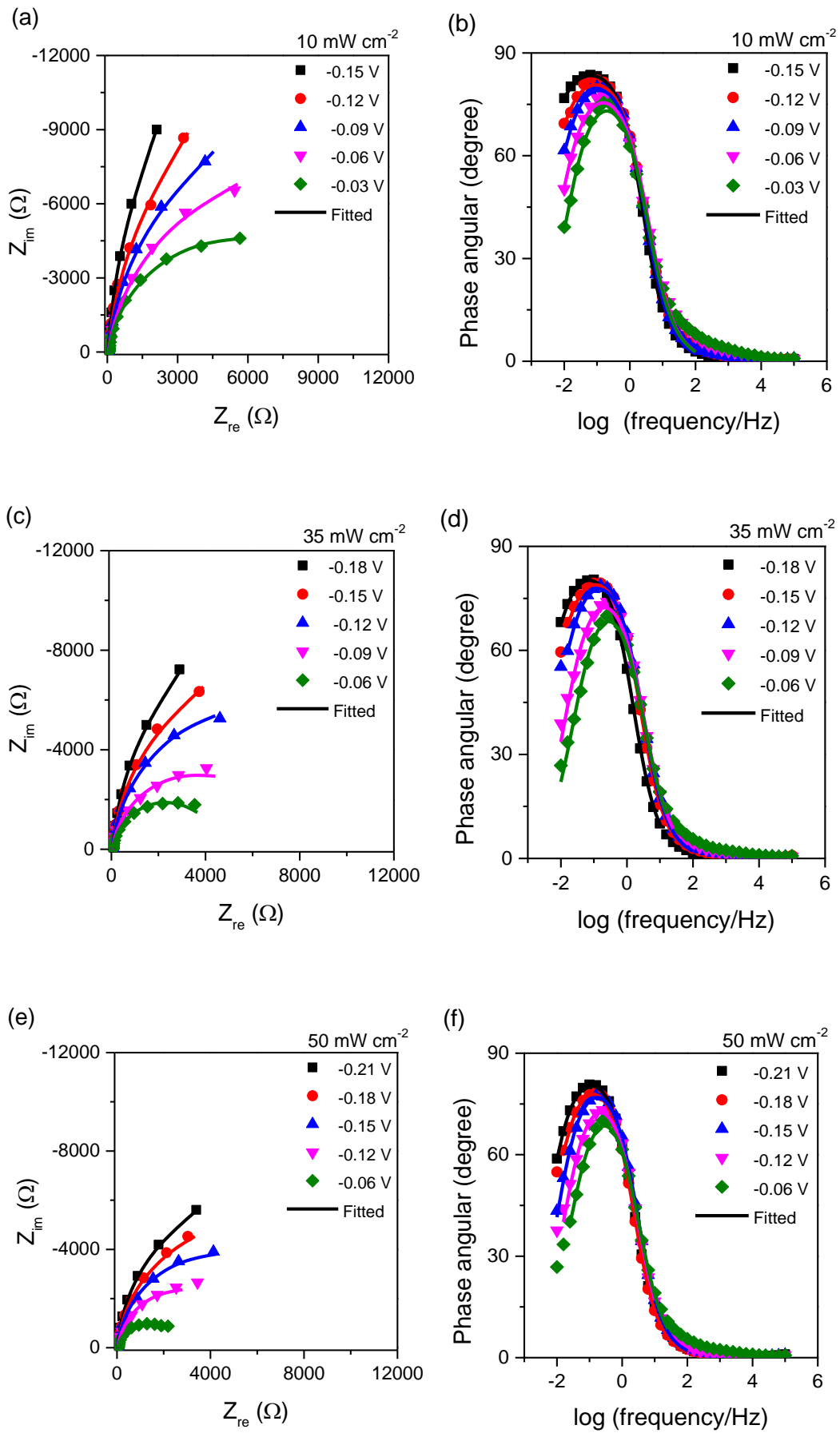
The photoelectrochemical performance of TiO<sub>2</sub> in the dark and various light intensities and solution pH were presented in **Figure S7 a-c**. It is shown that the increasing pH and light intensities lead to enhanced photocurrent which is defined as the difference in current between dark and illumination. The onset potential is also negatively shifted with them, in accordance with the photocurrent enhancement. In addition, the plateaued photocurrent under a corresponding high anodic potential at each pH is proportional to the light intensity, as shown in **Figure S7 d**, suggesting that the reaction dynamic is limited by the generation of photo-carriers rather than by the photooxidation of water as assumed.

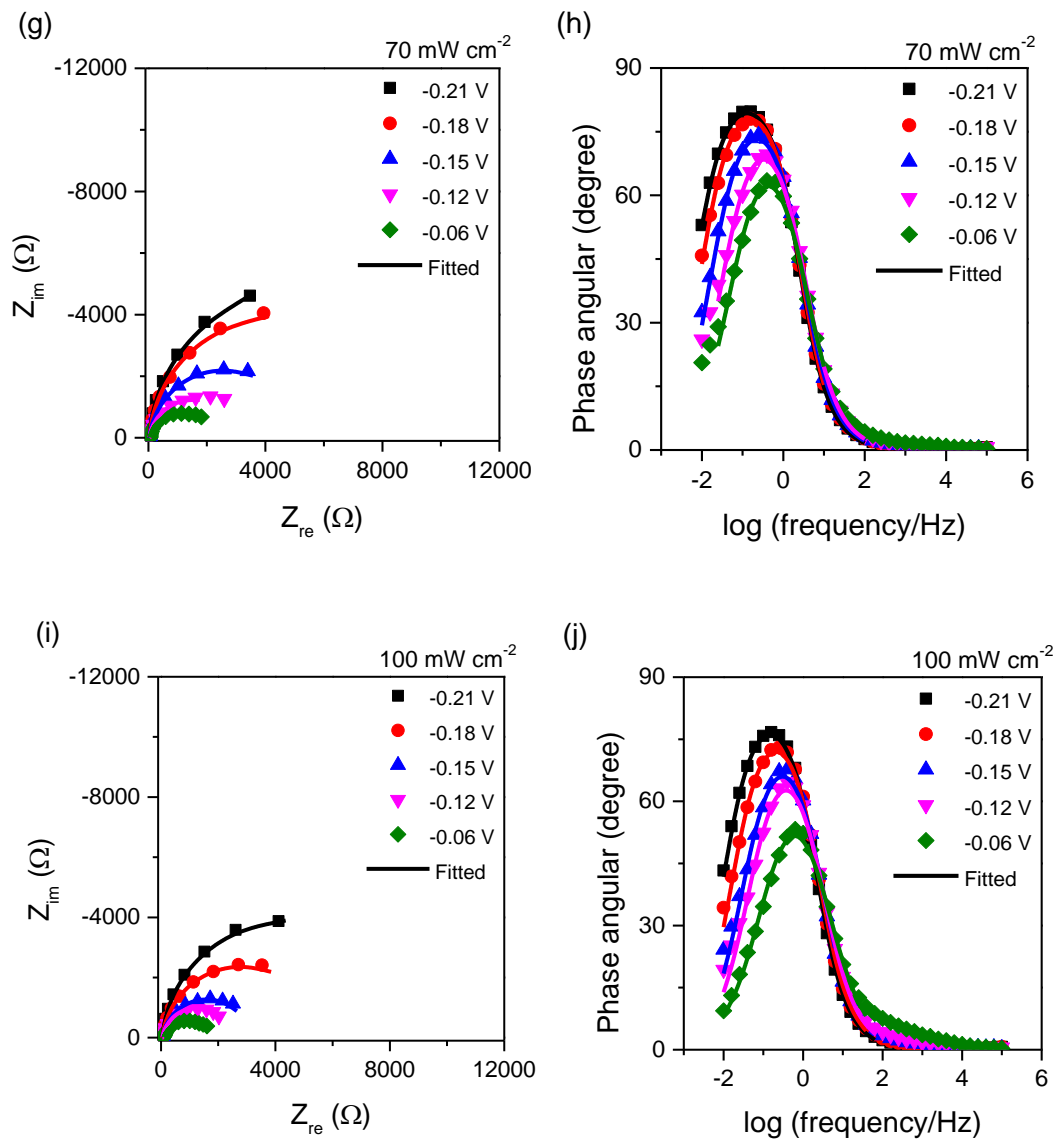


**Figure S7.** Current-potential curves for TiO<sub>2</sub> photoanode in deoxygenated electrolyte of different pH in the dark and under various light intensities: **a)** pH 2.<sup>30</sup> **b)** pH 6.6. **c)** pH 13.4; the scan rate was 10 mV s<sup>-1</sup>. **d)** the plateaued steady-state photocurrent for the electrodes at high anodic potential vs. light intensities, the measurements were recorded by stabilizing the photoanode for 60 s at the given potential (at 0.3, 0.1 -0.4 V<sub>SCE</sub> for pH 2.<sup>30</sup>, 6.6, 13.4, respectively).

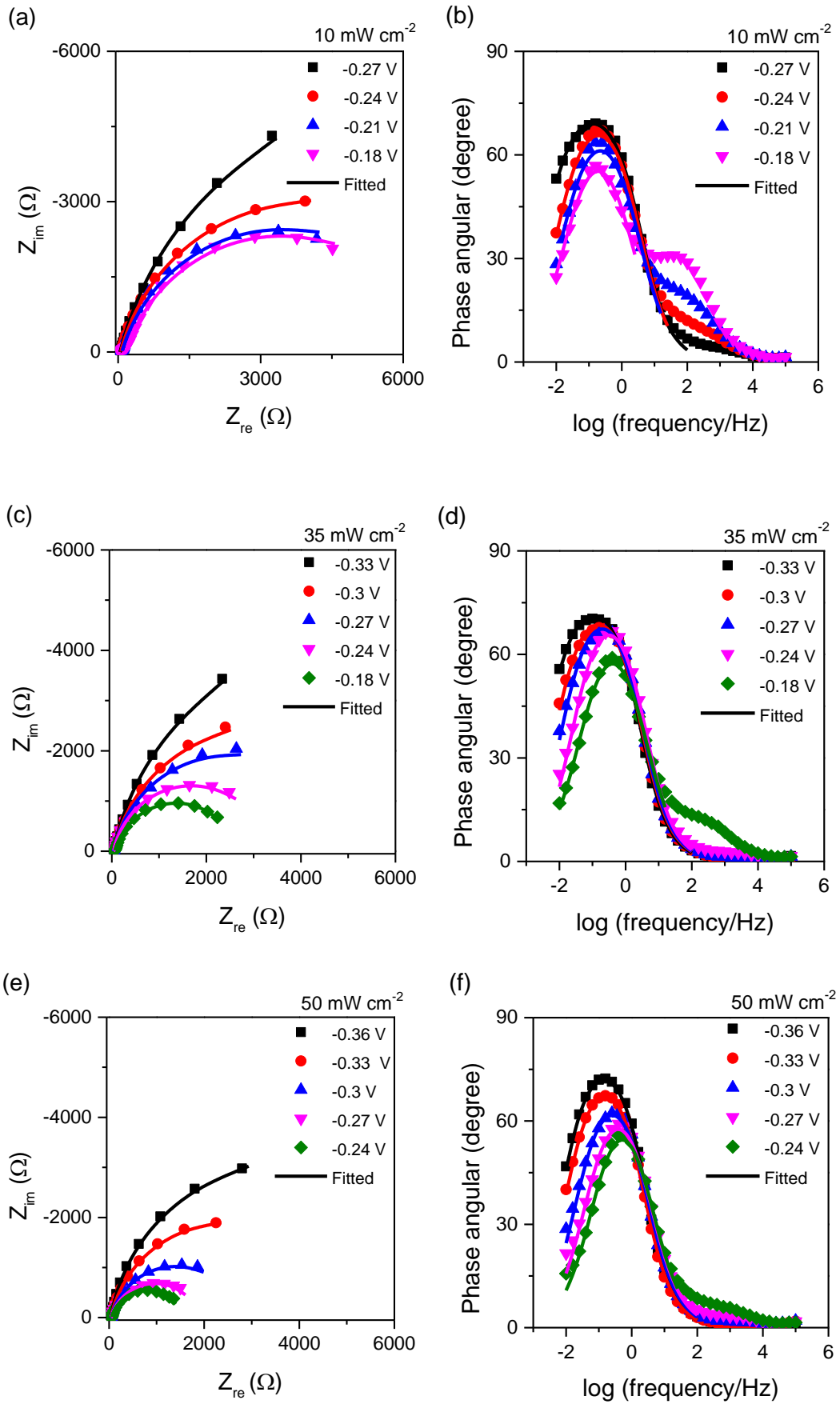
## 5.2 Electrochemical impedance spectroscopy (EIS) results

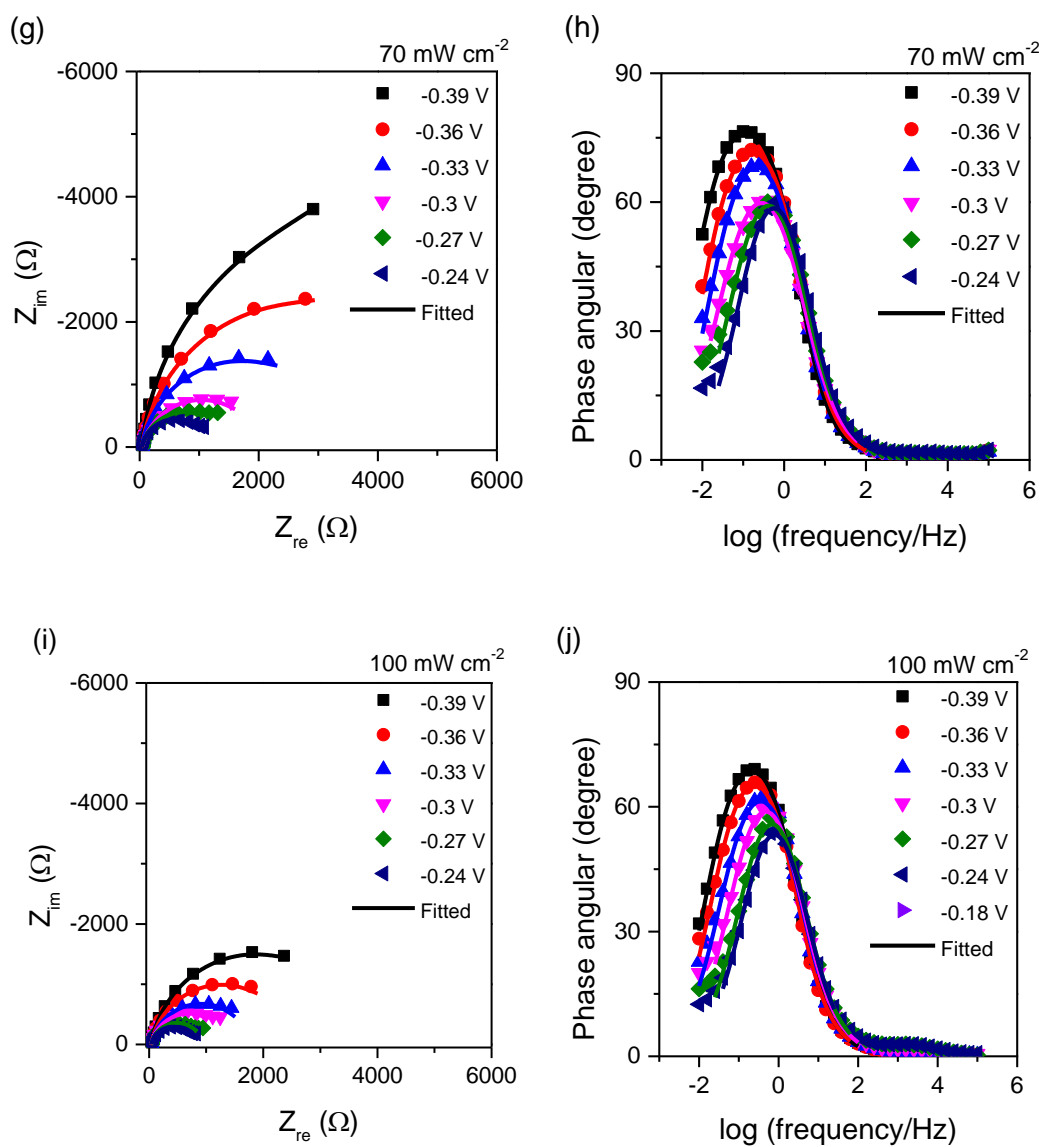
**Figure S8-10** is the typical EIS response of TiO<sub>2</sub> photoanode at various potential and light intensities in electrolyte of pH 2.0<sup>30</sup>, 6.6, and 13.4, respectively. In each case, only one semicircle arc and one peak were presented in the Nyquist plots and Bode plots. Note that the arc/peak at high frequency are almost identical to those measured in the dark where no photoelectrochemical reaction occurred. (see **Figure S6** and **Figure S10**). It is thus suggested that the arc/peak at high frequency does not represent the charge transfer process, but is associated with the combined space charge/surface state/oxide film capacitances and associated resistance. On the contrary, the arc/peak at low frequency obviously varies with light intensity and applied potential, alongside with only one time constant. This indicates that the arc/peak at low frequency can be assigned to photoelectrochemical reaction process. Moreover, these experimental results also agrees well with the simulation results of **eq. S13**, as shown in **Figure S8-10**. From the theoretic analysis of the EIS response<sup>15</sup>, the reason that high frequency arc/peak is not observed is probably due to the fact that the time constant of the first circle is too small to be detected under the tested frequency domain. This also indicates that the impedance of surface state will unlikely to affect EIS response at low frequency. Therefore we will focus on the analysis of EIS response at low frequency to derive rate constants.



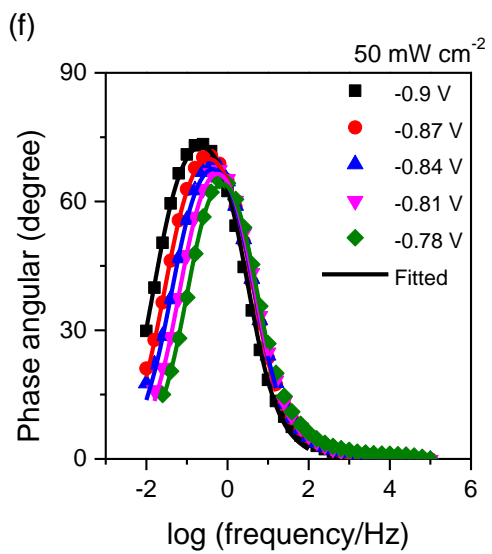
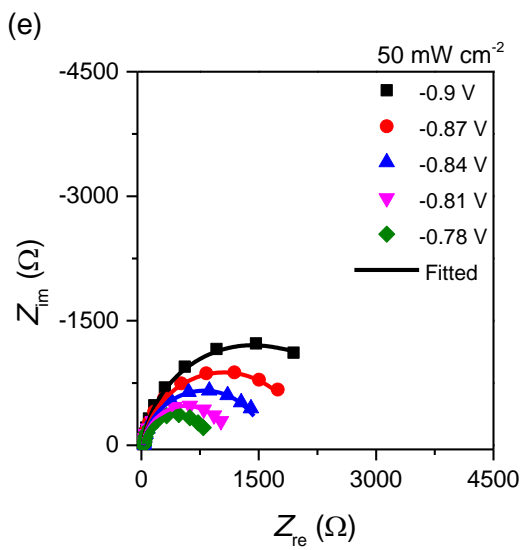
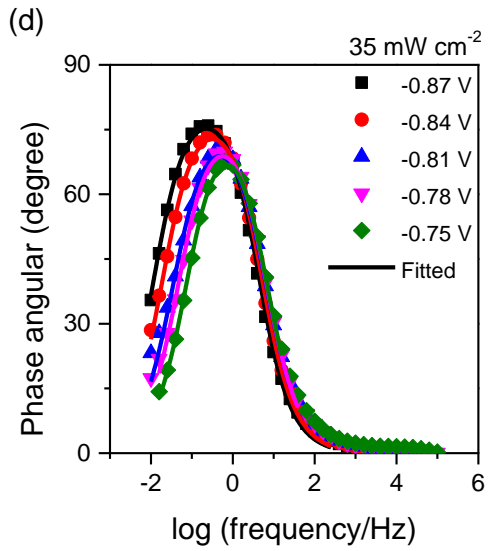
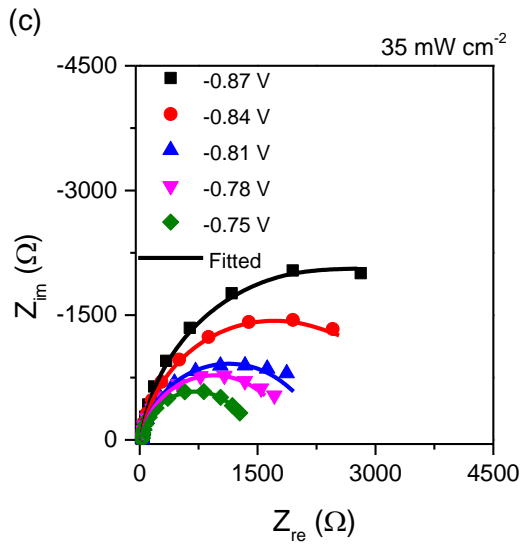
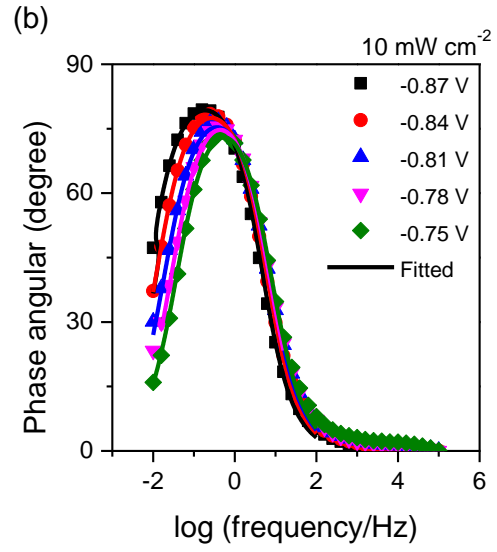
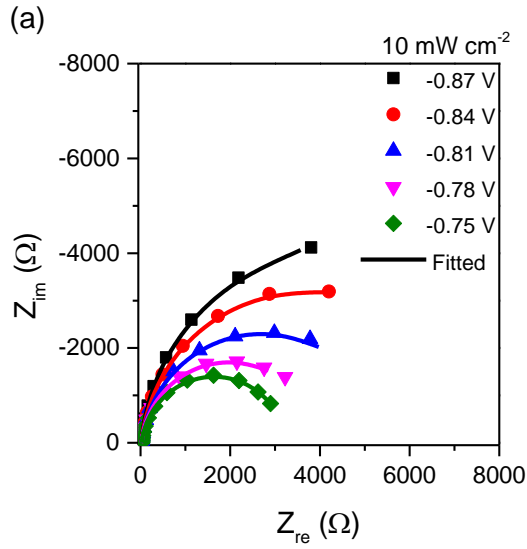


**Figure S8.** Typical EIS responses of TiO<sub>2</sub> photoanode in the deoxygenated electrolyte at pH 2.0 under different light intensities<sup>30</sup>: **a), c), e), g), i)** Nyquist plot. **b), d), f), h), j)** Bode plot.





**Figure S9.** Typical EIS responses of TiO<sub>2</sub> photoanode in the deoxygenated electrolyte at pH 6.6 under different light intensities: **a), c), e), g), i)** Nyquist plot. **b), d), f), h), j)** Bode plot.



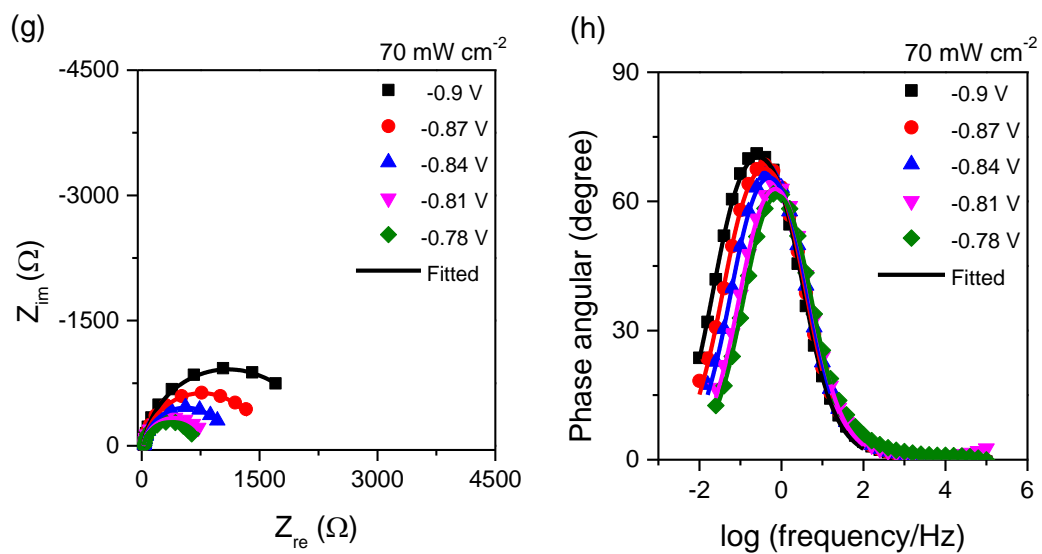
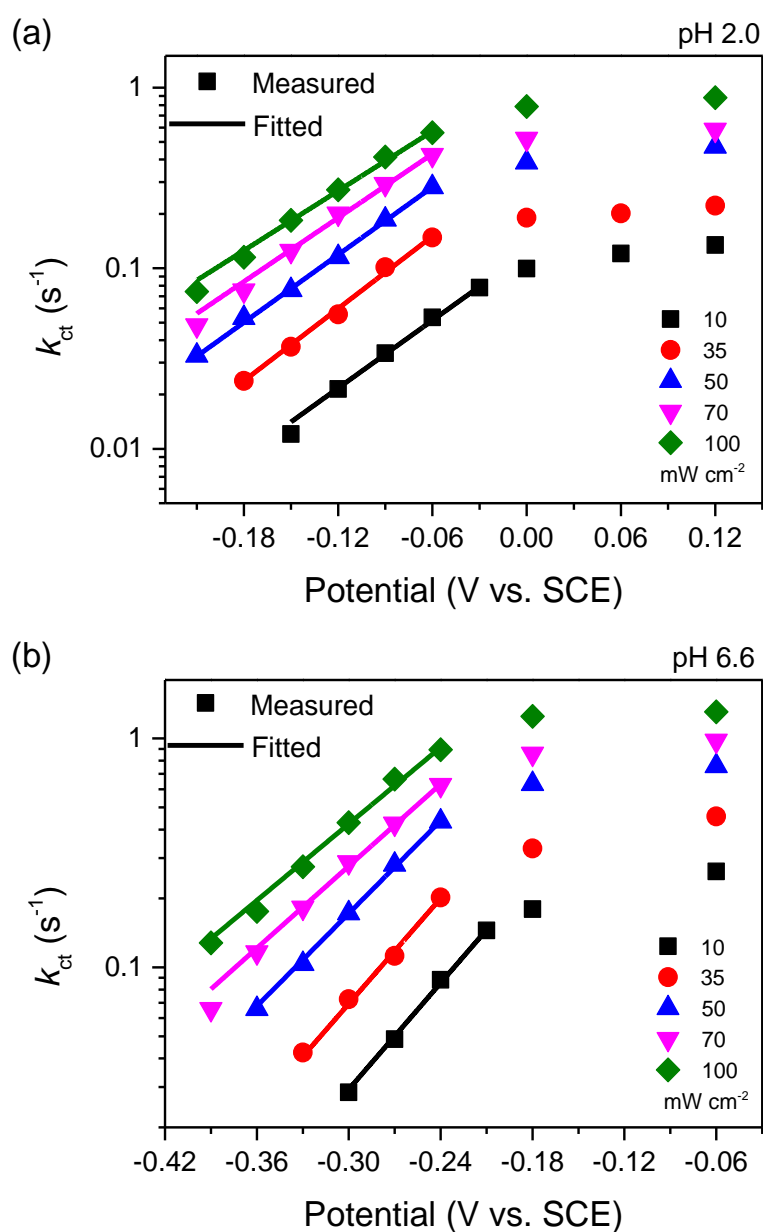


**Figure S10.** Typical EIS responses of TiO<sub>2</sub> photoanode in the deoxygenated electrolyte at pH 13.4 under different light intensities: **a), c), e), g)** Nyquist plot. **b), d), f), h)** Bode plot.

### 5.3 Derivation of $\omega_{\max}^1$ ( $k_{\text{ct}}$ )

As stated above, the arc/peak at low frequency can be assigned to photoelectrochemical reaction process. Therefore, the angular frequency of the maximum imaginary component ( $\omega_{\max}^1$ ) of the low frequency arc, which is the time constant of charge transfer process, is equal to the apparent charge transfer rate constant  $k_{\text{ct}}$ . This relationship is supported by other reports<sup>8, 15, 24, 31</sup>. In general, there are three ways to derive  $\omega_{\max}^1$ . It is common to derive  $\omega_{\max}^1$  by equivalent circuit fitting, however, this method is problematic to assign the physical meaning to the elements<sup>13, 15</sup> and fails to distinguish the potential coupling between space charge layer and Helmholtz layer<sup>15</sup>, thus may lead to inaccuracy. Alternatively,  $\omega_{\max}^1$  can be directly determined from the measured maximum frequency if enough data points within the maximum frequency range are recorded. But the stability of the photoanode is extremely required for this method. Due to the limitations of aforementioned methods, the  $\omega_{\max}^1$  in this manuscript was obtained by the mathematic fitting of **eq. S13**. The results are shown in **Figure 3 c** and **Figure S11 a** and **b**, which is also close to the measured maximum angular frequency. The potential and/or light intensity dependent  $\omega_{\max}^1$  suggest that the dynamics of photohole at the SCLJ can be described appropriately by the proposed kinetic model, even for the potential independent  $\omega_{\max}^1$  at high anodic potential (**Figure 3c** and **Figure S11 a, b**). According to **eq. S14**, reasons for this independence may be two folds: **1)** the  $C_{\text{SC}}$  is further decreased at high anodic potential; **2)** faster  $k_{\text{ct}}$  at high anodic potential accelerates photohole transfer, which results in decreased accumulation of photoholes. Together, these lead to reduced

increase in the amplitude of  $\phi_H$ , consequently resulting in the less potential dependent  $k_{ct}$ . Besides, as shown in **Figure S11 c**, a good linear correlation between  $\omega_{max}^1$  and  $j_{st}$  was observed at strong light intensity of  $100 \text{ mW cm}^{-2}$ , consistent with the theoretic prediction of the kinetic model (**eq. S16**). From the slope of  $\omega_{max}^1$  vs.  $j_{st}$  curve, the  $C_H$  for  $\text{TiO}_2$  photoanode are determined to be 1.23, 1.66, 2.59 mF for pH 2.0<sup>30</sup>, 6.6, and 13.4, respectively. The fitted results of  $\omega_{max}^1$  vs.  $j_{st}$  curve were listed in **Table S1**.



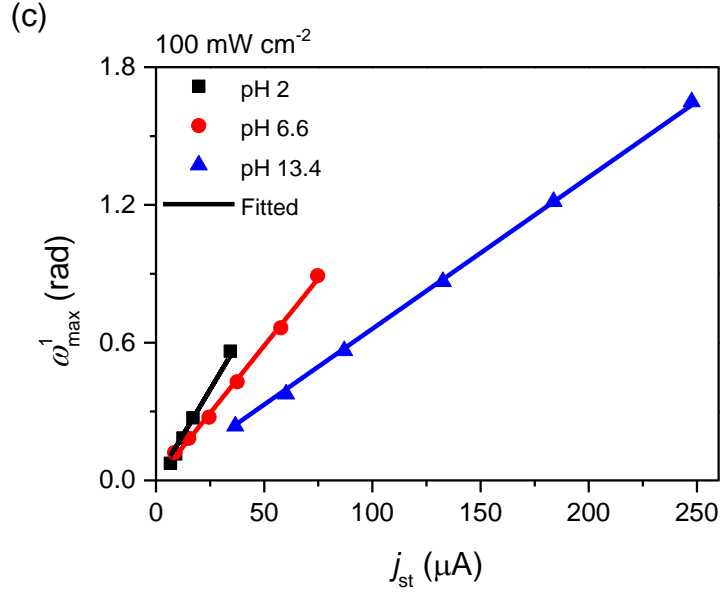


**Figure S11.** Influence of potential and light intensity (10, 35, 50, 70, 100 mW cm<sup>-2</sup>) on  $\omega_{max}^1$  ( $k_{ct}$ ) of the TiO<sub>2</sub> photoanode in the deoxygenated electrolyte of different pH: **a)** pH 2.0<sup>30</sup>. **b)** pH 6.6. **c)** relationship of the  $\omega_{max}^1$  vs. the steady-state photocurrent  $j_{st}$  under high light intensity illumination in different pH 2.0<sup>30</sup>, 6.6, and 13.4.

**Table S1.** Fitted results of **Figure S11 c.**

pH	Fitted equation	R <sup>2</sup>	C <sub>H</sub> (mF)
2	$y=0.0158*x$	0.9933	1.23
6.6	$y=0.0117*x$	0.9992	1.66
13.4	$y=0.0066*x$	0.9998	2.59

## 5.4 Derivation of $k_{sr}$

As we stated in the **Theory background**, the apparent surface recombination rate constant  $k_{sr}$ , can be obtained either by mathematic fitting of **eq. S13**, or calculated ratio from **eq. S17**. We found that the  $k_{sr}$  value obtained from these two methods are very

similar.  $k_{sr}$  presented herein is by the latter method, as shown in **Figure 3 d** and **Figure**

**S12.**

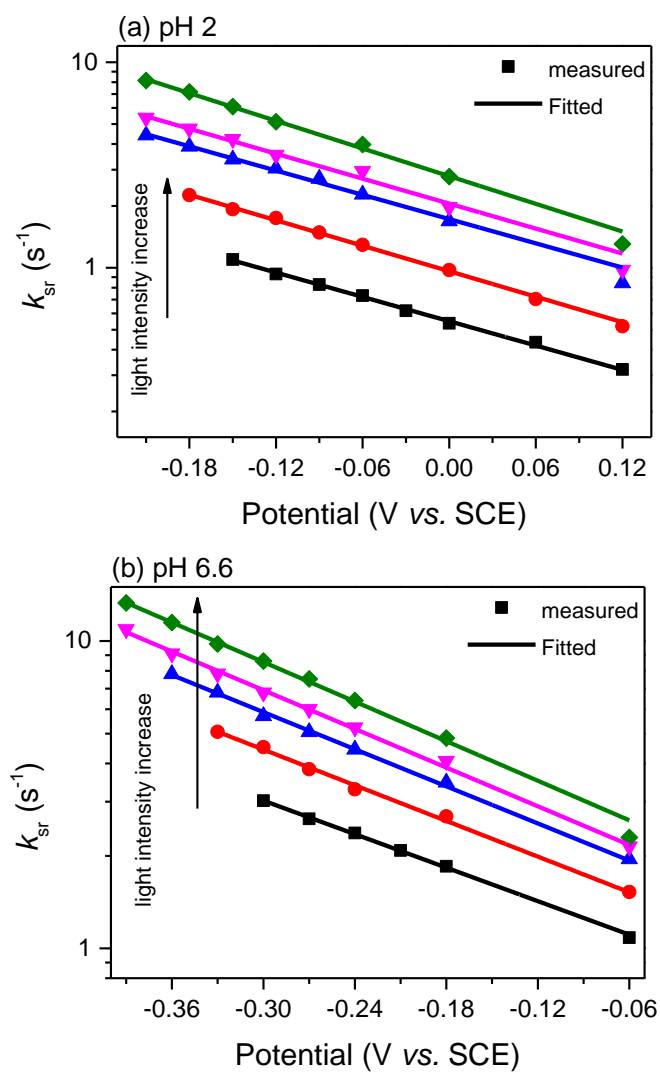


**Figure S12.** Influence of potential and light intensity (10, 35, 50, 70, 100  $mW\ cm^{-2}$ ) on the surface recombination rate constant ( $k_{sr}$ ) for the  $TiO_2$  photoanode in the deoxygenated electrolyte of different pH: **a)** pH 2.0. **b)** pH 6.6.

## 5.5 Fitted results of potential dependent rate constants

**Table S2.** Fitted results of the potential dependent  $k_{ct}$  and  $k_{sr}$  and the value of hole flux

$I_0$  under various light intensities at pH 2.0.

light intensity/ mW cm <sup>-2</sup>	Fitted equation	Fitted equation	$I_0$ /mA
10	$k_{ct}=0.12\exp(14.38*E)$	$k_{sr}=0.550\exp(-4.543*E)$	0.04
35	$k_{ct}=0.38\exp(15.36*E)$	$k_{sr}=0.962\exp(-4.757*E)$	0.085
50	$k_{ct}=0.67\exp(14.39*E)$	$k_{sr}=1.726\exp(-4.528*E)$	0.17
70	$k_{ct}=0.97\exp(13.57*E)$	$k_{sr}=2.052\exp(-4.660*E)$	0.22
100	$k_{ct}=1.23\exp(12.68*E)$	$k_{sr}=2.791\exp(-5.166*E)$	0.29

where  $E$  for the applied potential;  $E \leq -0.06$  V<sub>SCE</sub> for  $k_{ct}$

**Table S3.** Fitted results of the potential dependent  $k_{ct}$  and  $k_{sr}$  and the value of hole flux

$I_0$  under various light intensities at pH 6.6.

light intensity/ mW cm <sup>-2</sup>	Fitted equation	Fitted equation	$I_0$ /mA
10	$k_{ct}=6.17\exp(17.83*E)$	$k_{sr}=0.863\exp(-4.181*E)$	0.1
35	$k_{ct}=13.94\exp(17.68*E)$	$k_{sr}=4.265\exp(-4.677*E)$	0.24
50	$k_{ct}=18.17\exp(15.53*E)$	$k_{sr}=4.937\exp(-5.252*E)$	0.45
70	$k_{ct}=17.13\exp(13.75*E)$	$k_{sr}=5.895\exp(-5.453*E)$	0.55
100	$k_{ct}=19.86\exp(12.83*E)$	$k_{sr}=6.946\exp(-5.357*E)$	0.72

where  $E$  for the applied potential;  $E \leq -0.24$  V<sub>SCE</sub> for  $k_{ct}$

**Table S4.** Fitted results of the potential dependent  $k_{ct}$  and  $k_{sr}$  and the value of hole flux  $I_0$  under various light intensities at pH 13.4.

light intensity/ mW cm <sup>-2</sup>	Fitted equation	Fitted equation	$I_0$ /mA
10	$k_{ct}=4439.73\exp(12.83*E)$	$k_{sr}=0.0863\exp(-4.072*E)$	0.16
35	$k_{ct}=11742.63\exp(13.38* E)$	$k_{sr}=0.130\exp(-4.279*E)$	0.4
50	$k_{ct}=14238.26\exp(12.76* E)$	$k_{sr}=0.203\exp(-4.002*E)$	0.7
70	$k_{ct}=37043.81\exp(13.54* E)$	$k_{sr}=0.198\exp(-4.383*E)$	0.95
100	$k_{ct}=31746.66\exp(13.02* E)$	$k_{sr}=0.244\exp(-4.374*E)$	1.3

Where  $E$  for the applied potential;  $E \leq -0.78$  V<sub>SCE</sub> for  $k_{ct}$

## 5.6 Verification of $k_{ct}$ and $k_{sr}$

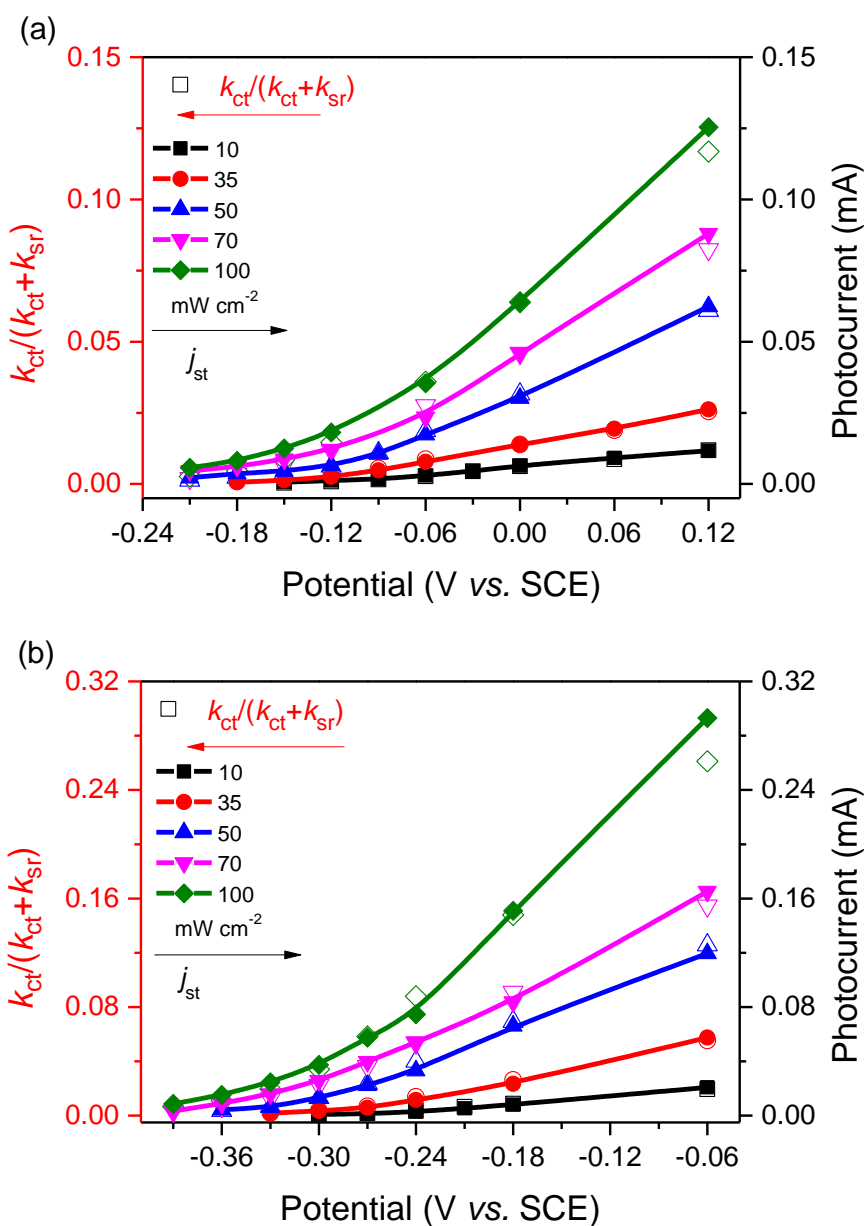


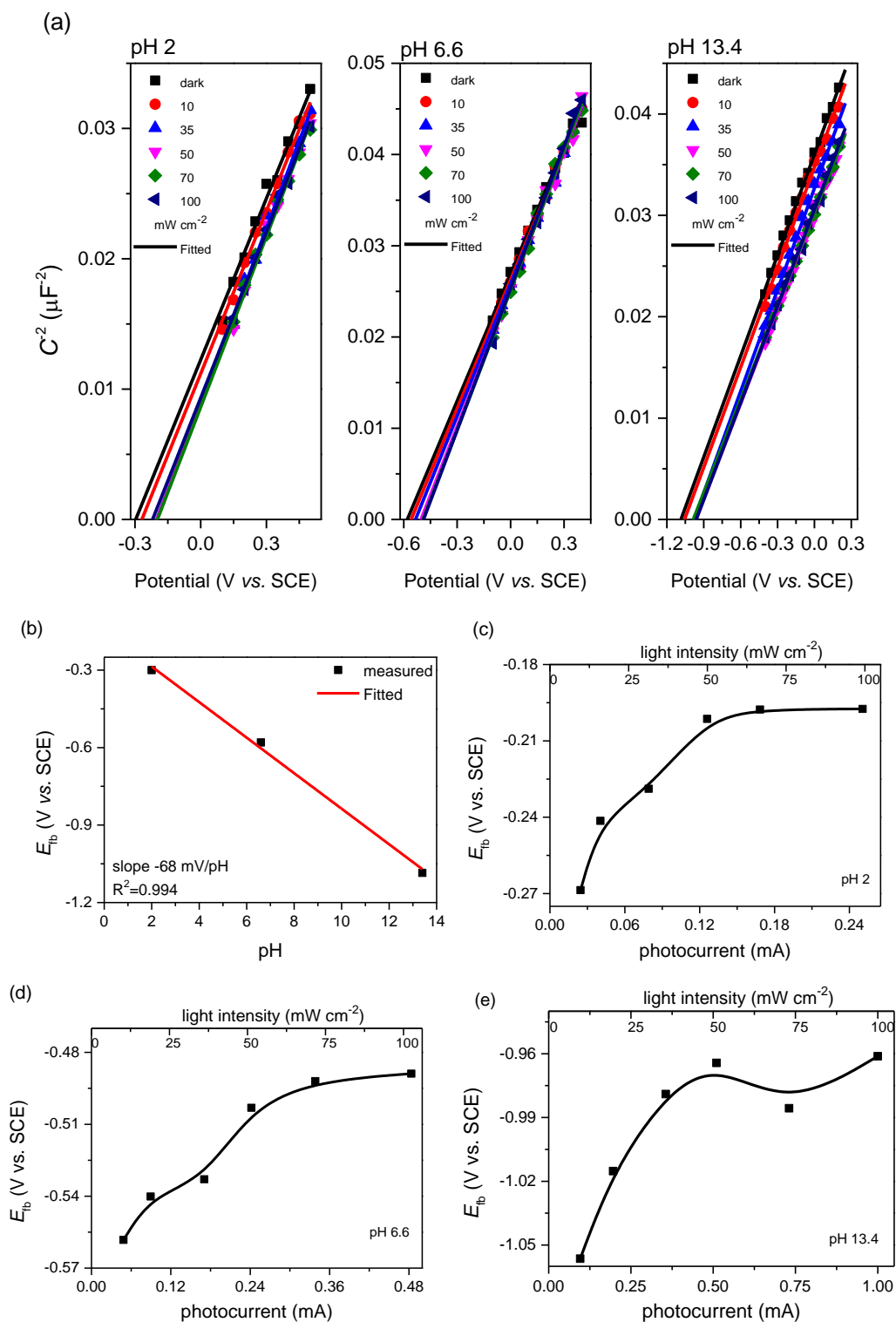
**Figure S13.** Comparison of steady-state photocurrent calculated by the ratio of  $k_{ct}/(k_{ct}+k_{sr})$  by eq. S9 and the measured values for the TiO<sub>2</sub> photoanode in the deoxygenated electrolyte: **a)** pH 2.0. **b)** pH 6.6.

## 5.7 Mott-Schottky measurements

To obtain flatband potential ( $E_{fb}$ ) of the TiO<sub>2</sub> photoanode, the Mott-Schottky

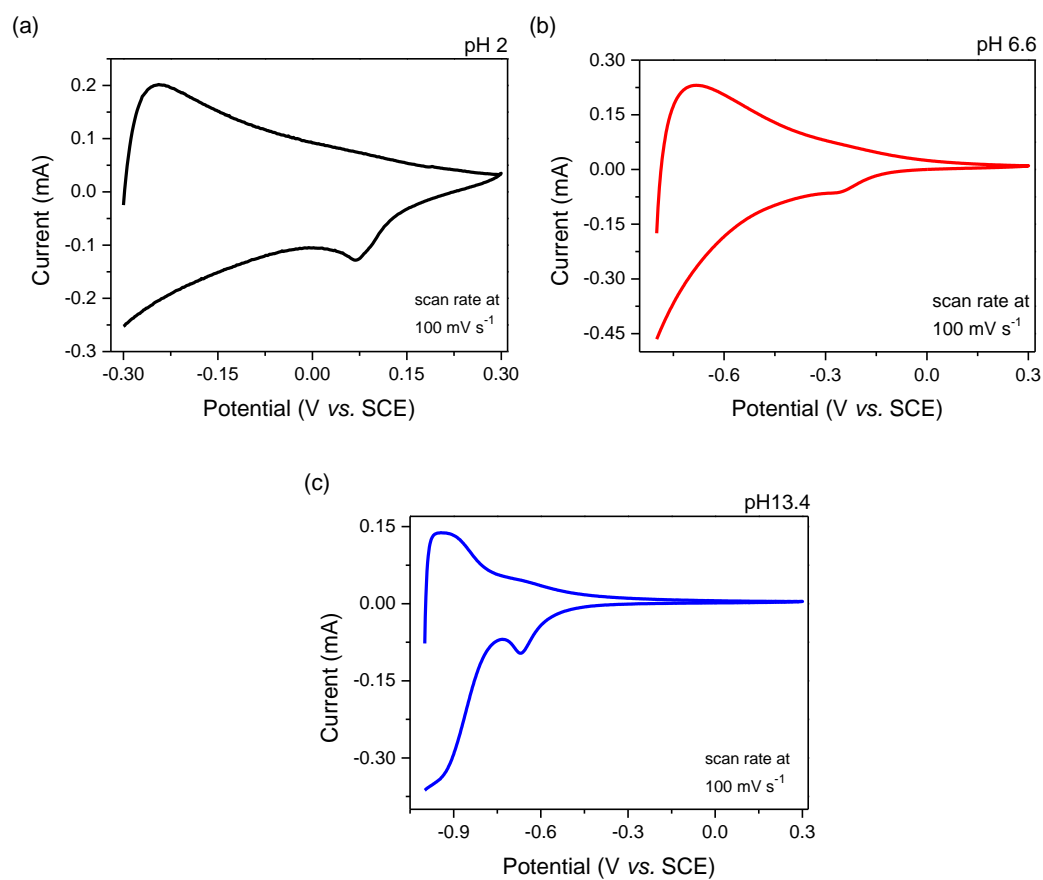
measurements were collected, as shown in **Figure S14 a**. The  $E_{fb}$  was obtained by linear fitting at high potentials of the M-S results. In the dark, the  $E_{fb}$  for TiO<sub>2</sub> photoanode are -1.08, -0.58, and -0.3 V<sub>SCE</sub> for pH 13.4, 6.6, and 2.0<sup>30</sup>, respectively. This result is in agreement with Nernstian equation with a slope of -68 mV/pH unit as shown in **Figure S14 b**, indicating that the electrode surface is covered by OH groups, in line with other reports.<sup>13, 31, 32</sup> Under illumination, the  $E_{fb}$  shifts positively as the light intensity increases and gradually saturated at high light intensity, as shown in **Figure S14 c-e**, manifesting that there are photooxidation intermediate trapped at the photoanode surface whose density is expected to increase with light intensity. This attribution is also supported by the presence of cathodic peak in cyclic voltammetry measurements (**Figure S15**) which is reported to be the oxidized intermediates on the photoanode surface.<sup>15, 33</sup> In addition, the plateau region at high light intensity suggests a limitation for the density of trapped photoholes at the photoanode surface. If we assume  $C_H$  equals to 5.90 mF cm<sup>-2</sup>, according to **eq. S26**, the maximum density of the trapped photoholes is calculated to be  $3.69 \times 10^{15}$  cm<sup>-2</sup>, given that the maximum shift of the  $E_{fb}$  is  $\sim 0.1$  V<sub>SCE</sub>.

$$dE_{fb} = -d\phi_H = \frac{qN_{trap}}{C_H} \quad (S26)$$



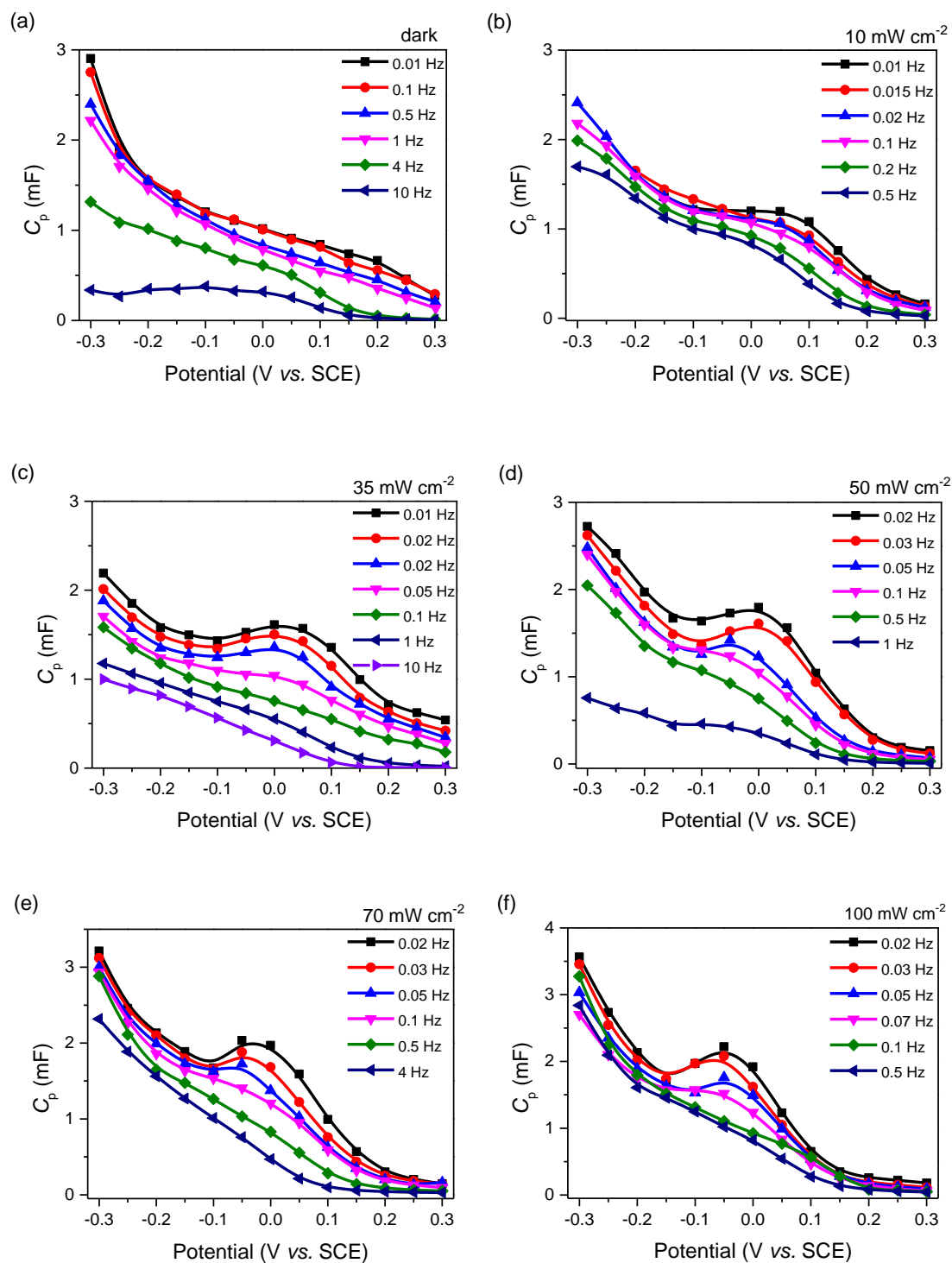
**Figure S14. a)** Mott-Schottky plots of the TiO<sub>2</sub> photoanode in the dark and under various light intensities, measured at 10 kHz. **b)** the pH dependence of the flatband potential in the dark, the relationship of flatband potential with various light intensities and saturated photocurrent density: **c)** pH 2.0<sup>30</sup>. **d)** pH 6.6. **e)** pH 13.4.

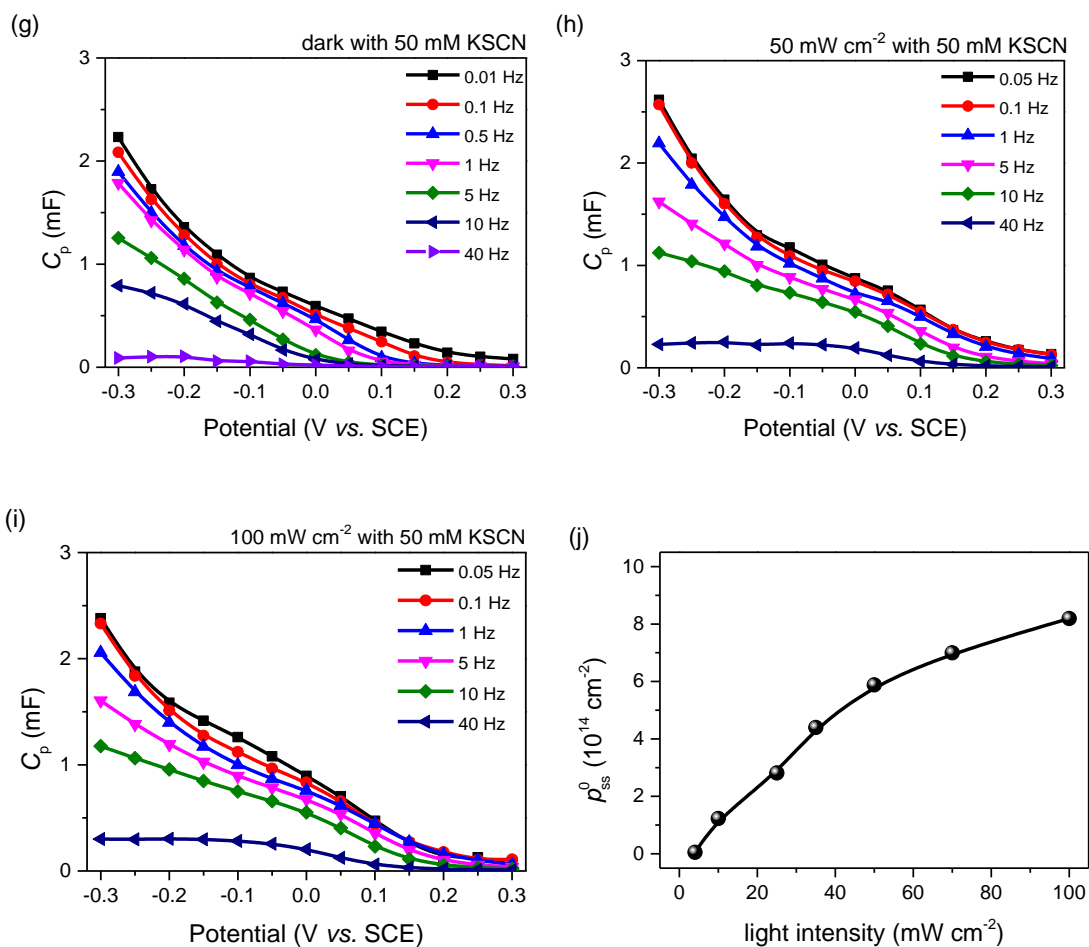
## 5.8 Cyclic voltammetry (CV) measurements



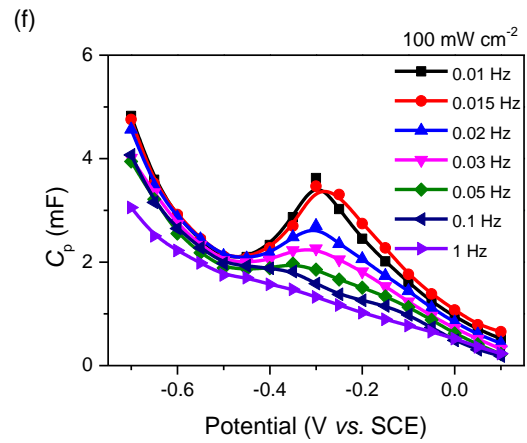
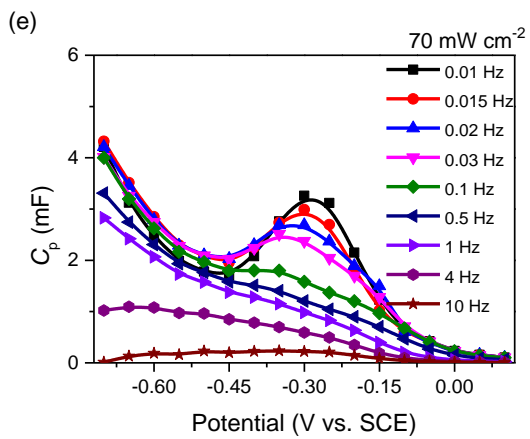
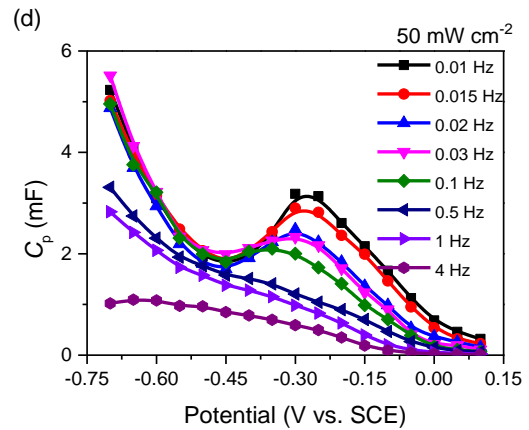
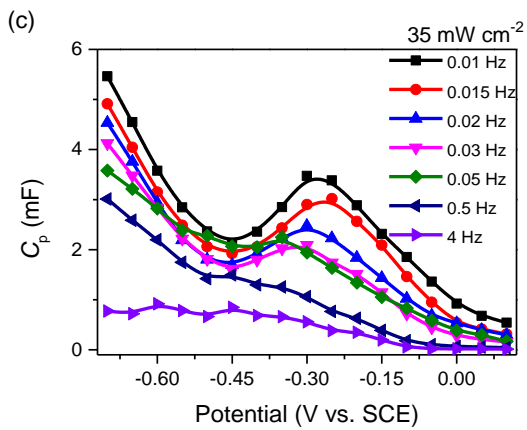
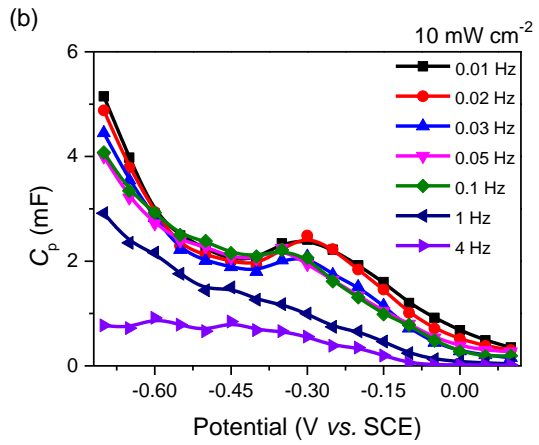
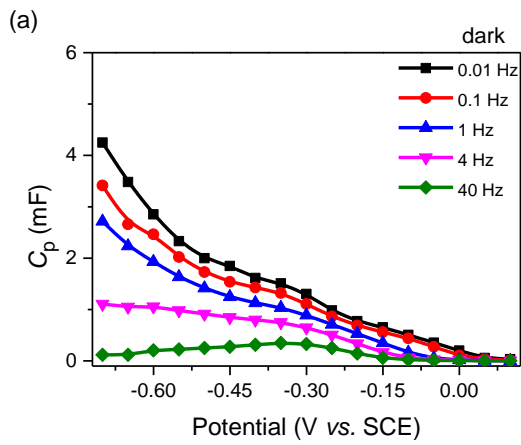
**Figure S15.** The cyclic voltammetry (CV) curves scanned at  $0.1 \text{ V s}^{-1}$  in the dark after the irradiation of 15 min: **a)** pH 2.0. **b)** pH 6.6. **c)** pH 13.4.

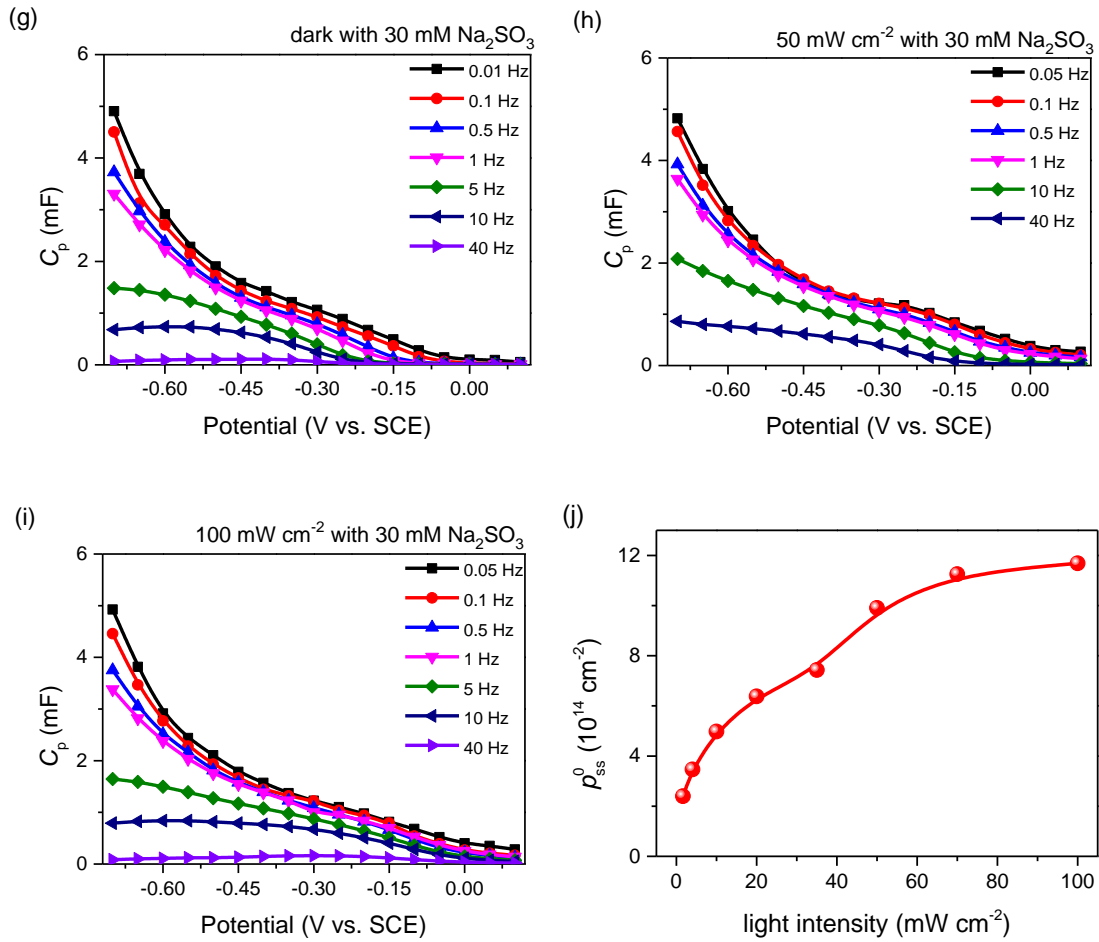
## 5.9 Bandgap states measurements



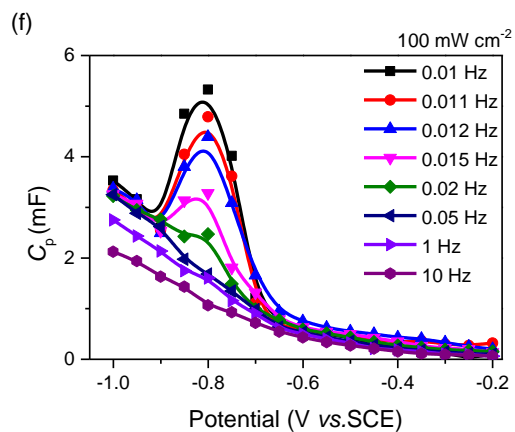
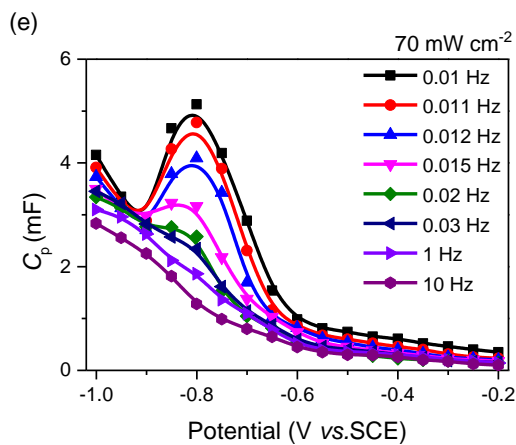
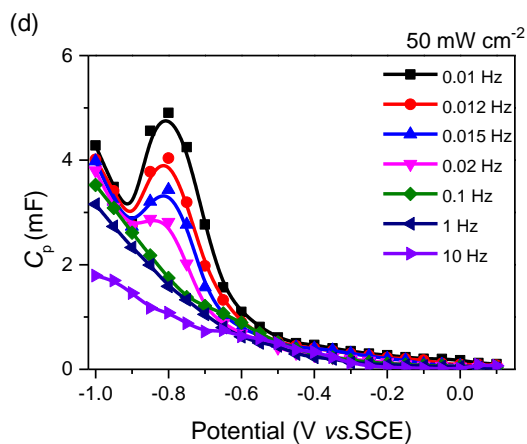
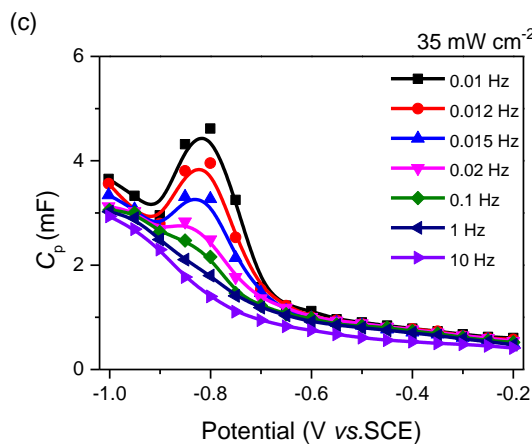
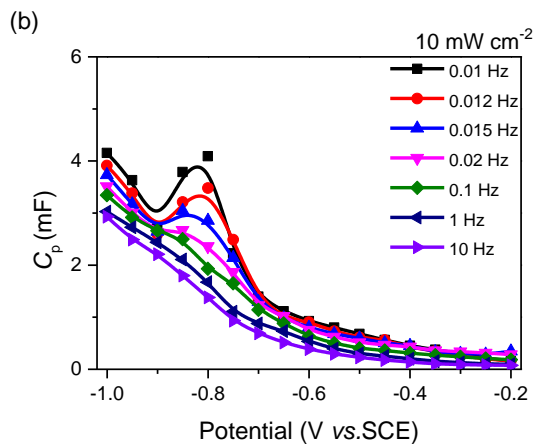
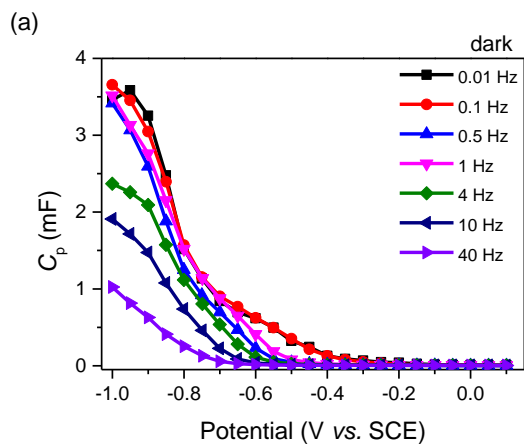


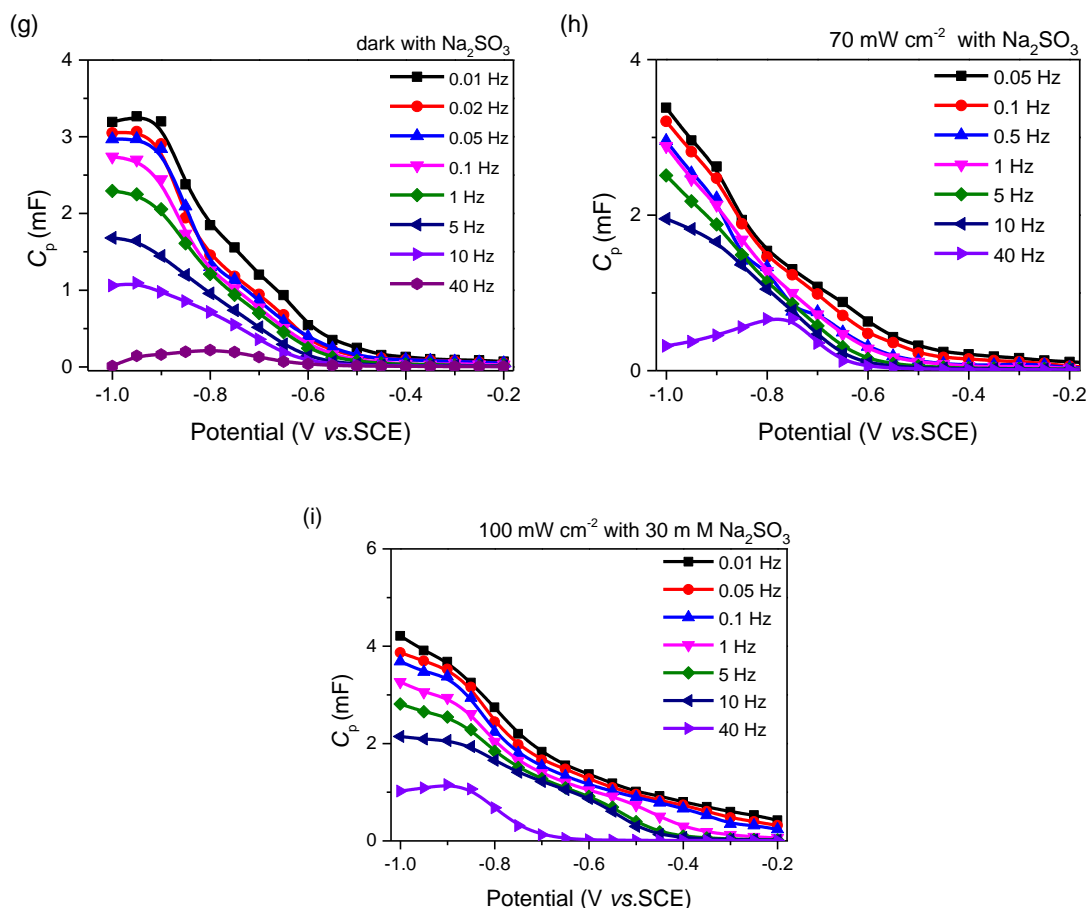
**Figure S16.** Steady-state photohole density derivation of TiO<sub>2</sub> photoanode at pH 2.0<sup>30</sup>. **a-f)** curves of pseudo-capacitance  $C_p(E_{\text{appl}}, \omega)$ -potential in the dark and various light intensities (10, 35, 50, 70, 100 mW cm<sup>-2</sup>). **g-i)** with the addition of 50 mM KSCN in the dark and various light intensities (50, 100 mW cm<sup>-2</sup>). **j)** the steady state density of the surface accumulated photohole  $p_{ss}^0$  under various light intensities (4, 10, 20, 35, 50, 70, 100 mW cm<sup>-2</sup>), which is calculated by eq. S25.





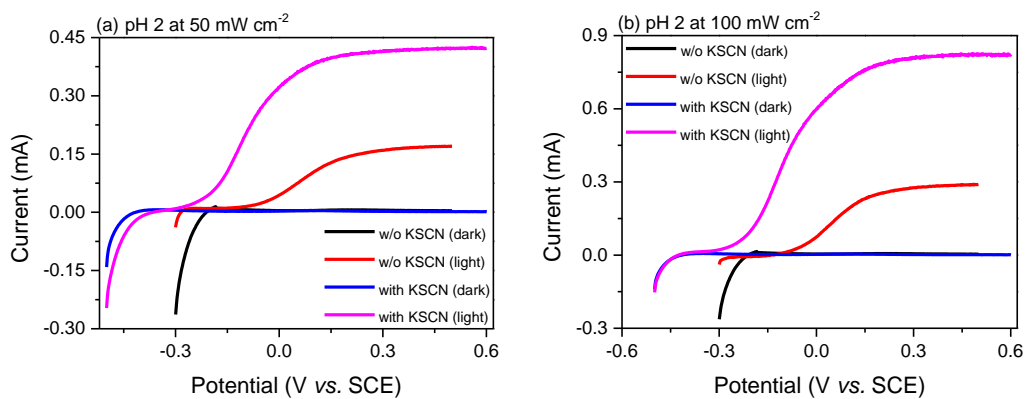
**Figure S17.** Steady-state photohole density derivation of  $\text{TiO}_2$  photoanode at pH 6.6. **a-f)** curves of pseudo-capacitance  $C_p(E_{\text{appl}}, \omega)$ -potential in the dark and various light intensities (10, 35, 50, 70, 100  $\text{mW cm}^{-2}$ ). **g-i)** with the addition of 30 mM  $\text{Na}_2\text{SO}_3$  in the dark and various light intensities (50, 100  $\text{mW cm}^{-2}$ ). **j)** the steady state density of the surface accumulated photohole  $p_{ss}^0$  under various light intensities (1.62, 4, 10, 20, 35, 50, 70, 100  $\text{mW cm}^{-2}$ ), which is calculated by **eq. S25**.





**Figure S18.** Steady-state photohole density derivation of  $\text{TiO}_2$  photoanode at pH 13.4. **a)-f)** curves of pseudo-capacitance  $C_p(E_{\text{appl}}, \omega)$ -potential in the dark and various light intensities (10, 35, 50, 70, 100  $\text{mW cm}^{-2}$ ). **g)-i)** with the addition of 30 mM  $\text{Na}_2\text{SO}_3$  in the dark and various light intensities (70, 100  $\text{mW cm}^{-2}$ ).

## 5.10 *I-V* curves at the presence of hole scavengers



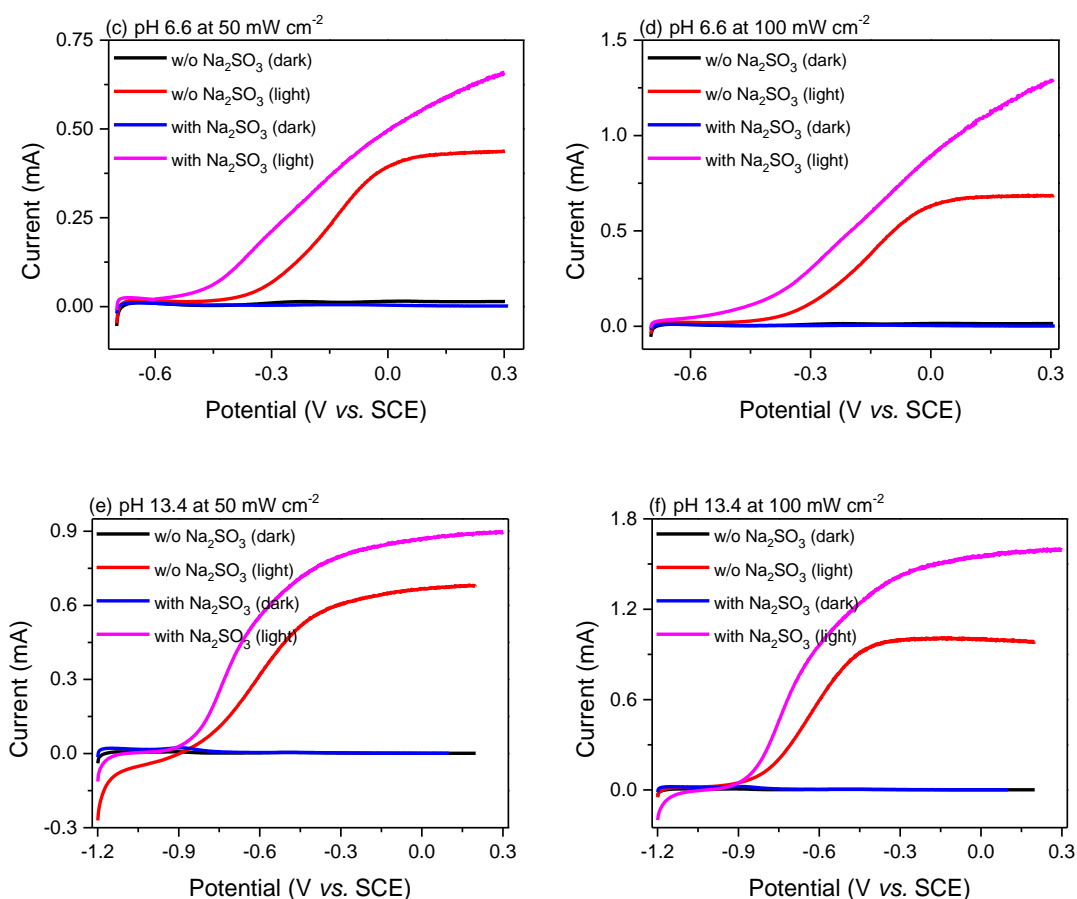


**Figure S19.** *I-V* curves of the TiO<sub>2</sub> photoanode with and without hole scavenger in the dark and under illumination, with and without 50 mM KSCN in **a)** 50 mW cm<sup>-2</sup> and **b)** 100 mW cm<sup>-2</sup> at pH 2.0, with and without 30 mM Na<sub>2</sub>SO<sub>3</sub> in **c)** 50 mW cm<sup>-2</sup> and **d)** 100 mW cm<sup>-2</sup> at pH 6.6, with and without 30 mM Na<sub>2</sub>SO<sub>3</sub> in **e)** 70 mW cm<sup>-2</sup> and **f)** 100 mW cm<sup>-2</sup> at pH 13.4.

## 5.11 Comparison of measured and calculated photocurrent

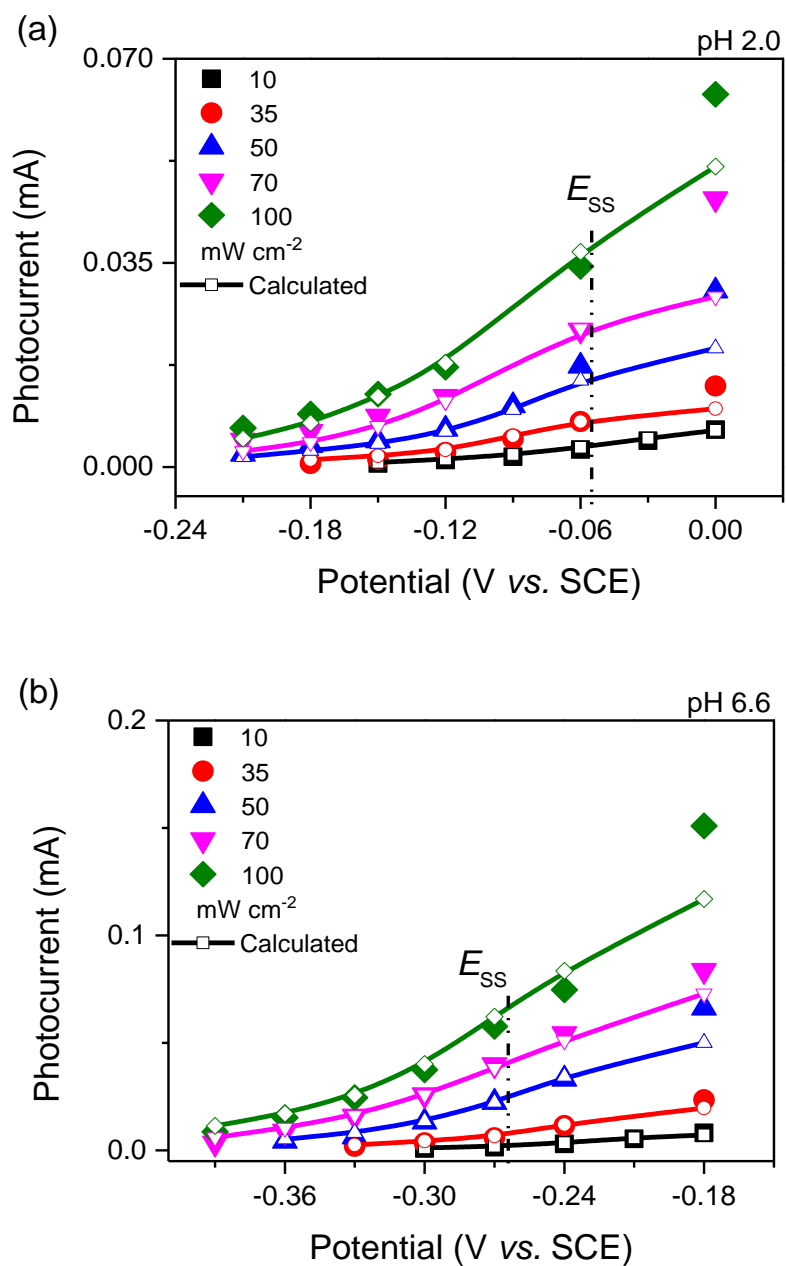


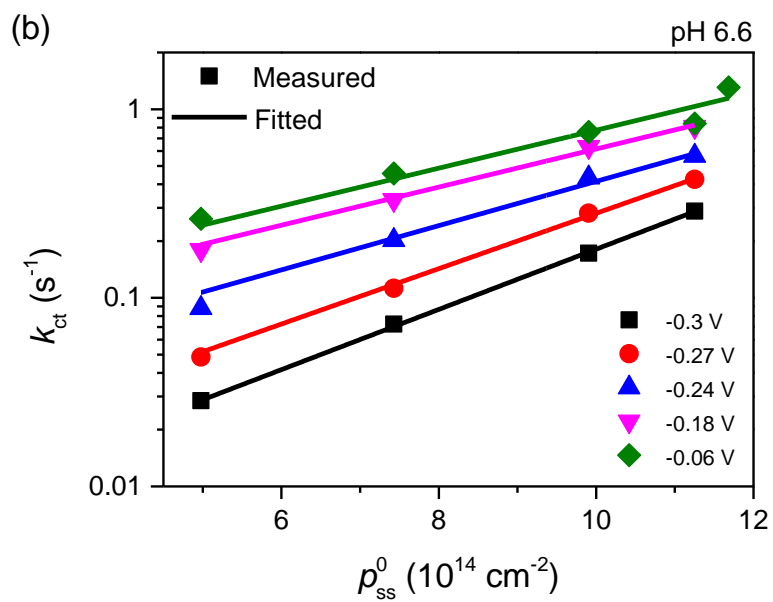
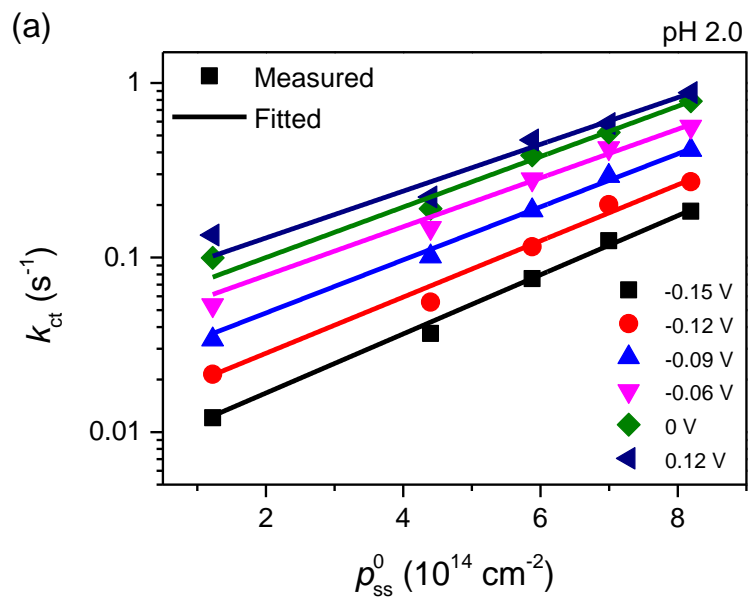
**Figure S20.** Comparison of measured steady-state photocurrent with that calculated by the product of  $k_{ct}$  and  $p_{ss}^0$  by eq. S9: **a)** pH 2.0<sup>30</sup>. **b)** pH 6.6.

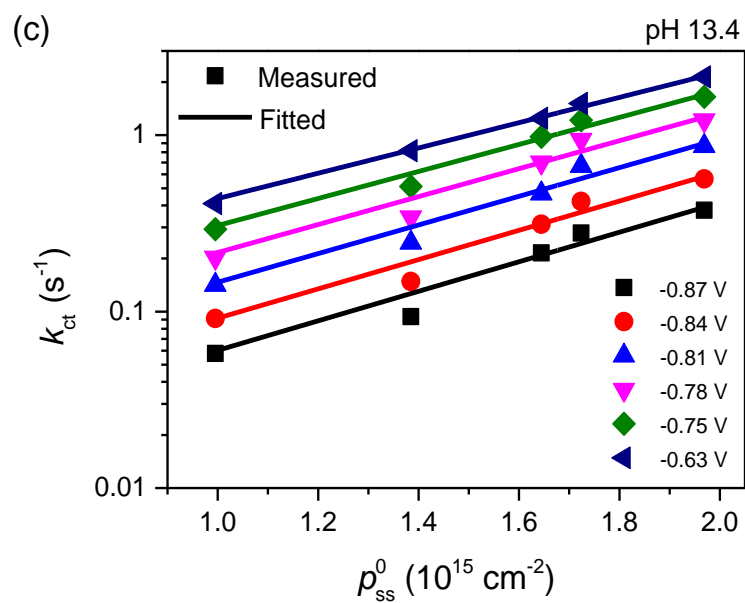
## 5.12 Relationship of $k_{ct}$ and $k_{sr}$ with surface hole density $p_{ss}^0$

As demonstrated in the main text, the  $\omega_{max}^1$  is light intensity dependent (**Figure 3 c** and **Figure S11 a, b**). According to our kinetic model<sup>7</sup>, this observation can be primarily attributed to the additional potential drop in Helmholtz layer ( $\Delta\varphi_H$ ) resulted from the accumulation of photohole on the photoanode surface, as predicted by **eq. S14**. In this case, the total potential drop in Helmholtz layer  $\varphi_H$  is the sum of 2 parts: **a)**  $\varphi_H^0$ , the inherent part, which is normally determined by the ratio of  $C_{SC}/C_H$ ; **b)**  $\Delta\varphi_H$  resulted from the accumulation of photohole  $p_{ss}^0$ , which can be written as  $\Delta\varphi_H = \frac{qp_{ss}^0}{C_H}$ . According to **eq. S5**,  $k_{ct}$  can be described by **eq. S27**.

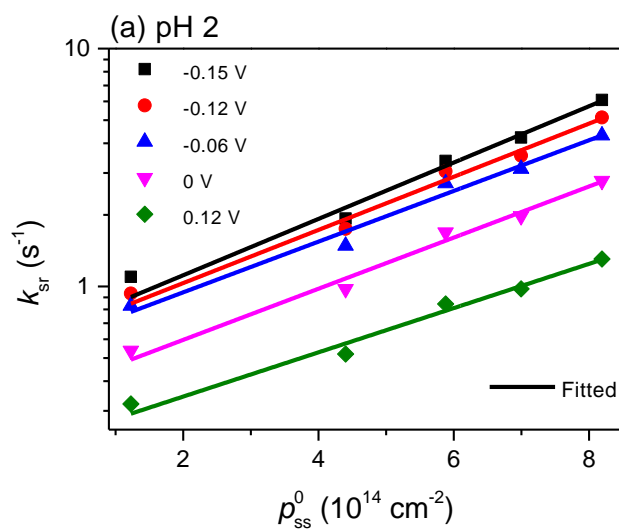
$$k_{ct} = k_{ct}^0 \exp\left(\frac{\beta q \varphi_H}{\kappa_B T}\right) = k_{ct}^0 \exp\left(\frac{\beta q \varphi_H^0}{\kappa_B T}\right) \exp\left(\frac{\beta q^2 p_{ss}^0}{\kappa_B T C_H}\right) \quad (\text{S27})$$

The  $\varphi_H^0$  is a constant at any given applied potential because the ratio of  $C_{SC}/C_H$  is fixed value. Thus a linear relationship of  $\ln k_{ct}$  vs.  $p_{ss}^0$  is expected. As shown in **Figure S21**, the  $\ln k_{ct}$  and  $p_{ss}^0$  is indeed proportional as predicted. Meanwhile, since the applied potential is held constant, the increase in  $\varphi_H$  resulted by  $p_{ss}^0$  will lead to the decrease in  $\varphi_{SC}$  by the same amount (i.e.  $\Delta\varphi_H = |-\Delta\varphi_{SC}|$ ), hence, also accelerating surface recombination process, as shown in **Figure 3 d** and **Figure S12**. Similar relationship was observed for  $\ln k_{sr}$  vs.  $p_{ss}^0$ , as shown in **Figure S22**.





**Figure S21.** Linear dependence of  $\ln k_{ct}$  vs.  $p_{ss}^0$  for  $\text{TiO}_2$  photoanode in the deoxygenated electrolyte of different pH: **a)** pH 2.0<sup>30</sup>. **b)** pH 6.6. **c)** pH 13.4.



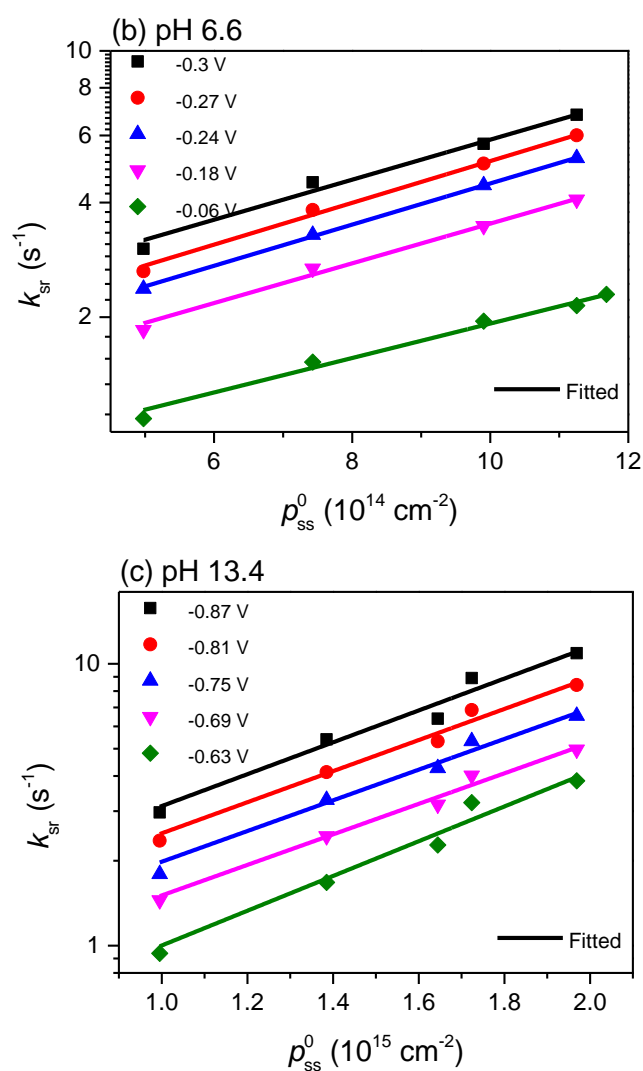


**Figure S22.** Linear dependence of  $\ln k_{sr}$  vs.  $p_{ss}^0$  for  $\text{TiO}_2$  photoanode in the deoxygenated electrolyte of different pH: **a)** pH 2.0. **b)** pH 6.6. **c)** pH 13.4.

## 6 Comparison with relevant work

Recently, several studies have been attempted to derive the *partial* parameters in rate law or expression. For instance, the rate order was derived to be 1 in the work of L. M. Peter *et al*<sup>6</sup> while the complete rate law is undetermined.

Durrant group<sup>1-5</sup> have reported rate law analysis on several metal oxide semiconductors. As stated above in the **section 1**, the reported rate law<sup>1</sup> could not

explain the nonlinear relationship between  $[h_s^+]$  and light intensity/photocurrent, and pH dependence of photocurrent. However, these controversies can be well explained by our rate law. More importantly, as we stated in the main text, the  $j_{st}$  vs.  $[h_s^+]$  data reported in the previous report<sup>1</sup> for TiO<sub>2</sub> can be well described by our rate equation (see **Figure S1 a**).

In our study, each kinetic parameters for the rate expression were independently obtained. The  $j_{st}$  was measured by the steady state technique. The  $k_{ct}$  was derived from electrochemical impedance spectroscopy (EIS) results by mathematic fitting (see **Figure 3c** and **Figure S11a-b**). The surface hole density accumulated on the surface states ( $p_{ss}^0$ ) are obtained by analyses of the impedance due to surface states (see **Figure 4b**, **Figure S16j** and **Figure S17j**). The correlation between the product of  $k_{ct}$  and  $p_{ss}^0$  with the measured  $j_{st}$  at the potential corresponding to the surface state energy level ( $E_{SS}$ ) demonstrate that the validity of our rate equation (see **Figure 4c** and **Figure S20**). Meanwhile, we stress that the measured  $j_{st}$  has never been used for the derivation of  $k_{ct}$  and  $n$ , thus we do not need other evidence to justify them. The reactant concentration dependence of rate law in terms of photocurrent was obtained by *varying* the light intensities (1.62~100 mW cm<sup>-2</sup>) with simultaneously measuring  $j_{st}$  and  $p_{ss}^0$  under a given applied potential. More  $j_{st}$ - $p_{ss}^0$  data at a wide range of  $p_{ss}^0$  (different light intensity) can be also described by our rate equation of **eq.3** as shown in **Figure 5a**. In particular, it is found that the  $k_{ct}$  is surface hole density dependent as described by **eq. S27**, which is the key difference between other reports<sup>1-5</sup> and ours. This phenomenon of a reactant concentration dependent rate constant is conceptually unexpected and

rarely reported in the literature. Unlike the conventional reactants, the accumulation of such high concentration photogenerated charge ( $10^{14}\sim 10^{15}$  cm<sup>-2</sup>) on the electrode surface will cause the applied potential redistribution between the space charge layer and the Helmholtz layer, and consequently affecting the activation energy during transfer across the interface of electrode/electrolyte (*partial Fermi level pinning*). Additionally, one of the possibilities that the rate order is greater than 1 may exist: if the light intensity increase beyond the range we studied, the hole transfer occurs via the valence band (free hole with identical energy) then the  $k_{ct}$  is constant. Under this circumstance, the rate order can be greater than 1 if the  $j_{st}$  is not *linearly* proportional to the density of surface free hole. But it is worth noting that no evidence can be proofed that it is the valence band holes detected through electric or optic measurements in the previous reports.<sup>1,6</sup>

**Table S5.** Comparison between the positive shift in  $E_{fb}$  under illumination and the change in  $\phi_H$  resulted by the accumulated photohole at 100 mW cm<sup>-2</sup>

pH	the shift of $E_{fb}$ (V vs. SCE)	$\Delta\phi_H$ resulted by the accumulated photohole (V vs. SCE)
2.0	0.0995	0.1602
6.6	0.0911	0.1692
13.4	0.1238	0.1821

## 7 Implication on kinetic study

As revealed in the manuscript, the water photo-oxidation rate is determined by the product of  $k_{ct}$  and  $p_{ss}^0$ , so they are both important for the photocurrent enhancement. To illustrate this relationship, as the horizontal line shows in **Figure 5 a**, similar  $j_{st}$  can be achieved by varying the light intensities for TiO<sub>2</sub> photoanode at different pH (100, 50, 20 mW cm<sup>-2</sup> light intensity for pH 2.0, 6.6 and 13.4, respectively). It has to be noted that even though  $p_{ss}^0$  is significantly lower at pH 2.0, it has greater  $k_{ct}$  due to higher light intensity. Meanwhile, similar  $p_{ss}^0$  can also be achieved at varies light intensities (>100, 50, 10 mW cm<sup>-2</sup> for pH 2.0, 6.6 and 13.4, respectively), as the vertical line shows in **Figure 5 a**. However,  $j_{st}$  varies due to  $k_{ct}$  variation at different light intensities. Moreover, these results suggest that light intensity plays the dominating role to determine reaction rate. As a matter of fact, the increased light intensity affects the environmental energy input for the reaction system, thus increase both  $p_{ss}^0$  and  $k_{ct}$ , leading to increased  $j_{st}$ .

Besides, our rate law analysis strongly indicates that the surface bound OH<sup>-</sup> is involved in the water photo-oxidation reaction, and the chemical nature of the surface state is likely to be the surface bound •OH during the initial step of photohole transfer. This is consistent with redox photooxidation mechanism proposed by Salvador *et. al.*<sup>34</sup>.

<sup>35</sup> A scheme to illustrate TiO<sub>2</sub> water photo-oxidation mechanism is depicted in **Figure S23**. Since a total of four photoholes are needed for the formation of O<sub>2</sub>, mechanistic investigation of three subsequent photohole transfer would require the help of spectroscopic measurements.

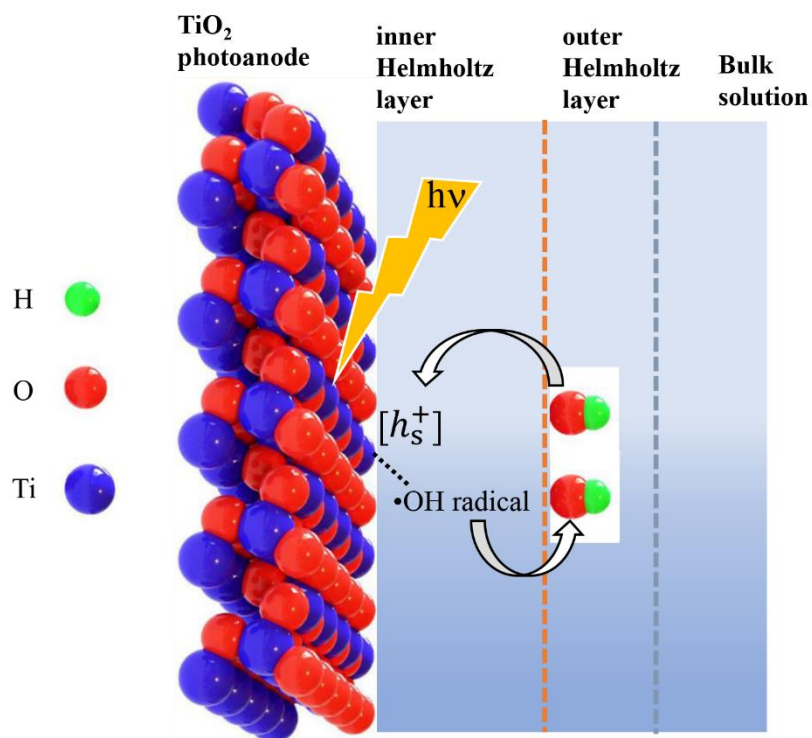


**Figure S23.** Schematic illustration of the water photo-oxidation mechanism on  $\text{TiO}_2$  photoanode.

## 8 Reference

1. A. Kafizas, Y. Ma, E. Pastor, S. R. Pendlebury, C. Mesa, L. Francàs, F. Le Formal, N. Noor, M. Ling, C. Sotelo-Vazquez, C. J. Carmalt, I. P. Parkin and J. R. Durrant, *ACS Catal.*, 2017, **7**, 4896-4903.
2. C. A. Mesa, L. Francas, K. R. Yang, P. Garrido-Barros, E. Pastor, Y. Ma, A. Kafizas, T. E. Rosser, M. T. Mayer, E. Reisner, M. Gratzel, V. S. Batista and J. R. Durrant, *Nat Chem*, 2020, **12**, 82-89.
3. F. Le Formal, E. Pastor, S. D. Tilley, C. A. Mesa, S. R. Pendlebury, M. Gratzel and J. R. Durrant, *J Am Chem Soc*, 2015, **137**, 6629-6637.
4. Y. Ma, C. A. Mesa, E. Pastor, A. Kafizas, L. Francàs, F. Le Formal, S. R. Pendlebury and J. R. Durrant, *ACS Energy Lett.*, 2016, **1**, 618-623.

5. J. Li, W. Wan, C. A. Triana, H. Chen, Y. Zhao, C. K. Mavrokefalos and G. R. Patzke, *Nat Commun*, 2021, **12**, 255.
6. L. M. Peter, A. B. Walker, T. Bein, A. G. Hufnagel and I. Kondofersky, *J. Electroanal. Chem.*, 2020, **872**.
7. S. Zhang and W. Leng, *Nat. Chem.*, 2020, DOI: 10.1038/s41557-020-00569-y.
8. K. G. Upul Wijayantha, S. Saremi-Yarahmadi and L. M. Peter, *Phys. Chem. Chem. Phys.*, 2011, **13**, 5264-5270.
9. G. Cooper, J. A. Turner and A. J. Nozik, *J. Electrochem. Soc.*, 1982, **129**, 1973-1977.
10. P. Salvador, *J. Electrochem. Soc.*, 1981, **128**, 1895-1900.
11. L. Peter, *Developments in Electrochemistry*, 2014, DOI: <https://doi.org/10.1002/9781118694404.ch18>, 331-347.
12. D. Tafalla and P. Salvador, *J. Electroanal. Chem. Interfacial Electrochem.*, 1989, **270**, 285-295.
13. H. Cachet and E. M. M. Sutter, *J. Phys. Chem. C*, 2015, **119**, 25548-25558.
14. C. A. Mesa, L. Francàs, K. R. Yang, P. Garrido-Barros, E. Pastor, Y. Ma, A. Kafizas, T. E. Rosser, M. T. Mayer, E. Reisner, M. Grätzel, V. S. Batista and J. R. Durrant, *Nat. Chem.*, 2020, **12**, 82-89.
15. W. H. Leng, Z. Zhang, J. Q. Zhang and C. N. Cao, *J. Phys. Chem. B*, 2005, **109**, 15008-15023.
16. L. M. Peter, A. B. Walker, T. Bein, A. G. Hufnagel and I. Kondofersky, *J. Electroanal. Chem.*, 2020, **872**, 114234.

17. B. Klahr, S. Gimenez, F. Fabregat-Santiago, T. Hamann and J. Bisquert, *J. Am. Chem. Soc.*, 2012, **134**, 4294-4302.
18. G. M. Carroll and D. R. Gamelin, *J. Mater. Chem. A*, 2016, **4**, 2986-2994.
19. D. J. Fermín, E. A. Ponomarev and L. M. Peter, *J. Electroanal. Chem.*, 1999, **473**, 192-203.
20. P. Shangguan, S. Tong, H. Li and W. Leng, *RSC Adv.*, 2013, **3**, 10163-10167.
21. J. C. S. G. Oskam, P. M. Hoffmann, P. C. Searson\*, *J. Electrochem. Soc.*, 1996, **143**, 2531-2537.
22. G. O. Peter M. Hoffmann, and Peter C. Searson, *J. Appl. Phys.*, 1998, **83**, 4309-4323.
23. S. Zhang, P. Shangguan, S. Tong, Z. Zhang and W. Leng, *J. Phys. Chem. C*, 2019, **123**, 24352-24361.
24. S. Zhang, Z. Zhang and W. Leng, *Phys. Chem. Chem. Phys.*, 2020, **22**, 7835-7843.
25. H. Tada and H. Honda, *J. Electrochem. Soc.*, 1995, **142**, 3438-3443.
26. W. H. Leng, W. C. Zhu, J. Ni, Z. Zhang, J. Q. Zhang and C. N. Cao, *Applied Catalysis A: General*, 2006, **300**, 24-35.
27. G. Ai, R. Mo, H. Li and J. Zhong, *Nanoscale*, 2015, **7**, 6722-6728.
28. C. Liu, C. Zhang, G. Yin, T. Zhang, W. Wang, G. Ou, H. Jin and Z. Chen, *ACS Appl Mater Interfaces*, 2021, **13**, 13301-13310.
29. H. Fei, W. Leng, X. Li, X. Cheng, Y. Xu, J. Zhang and C. Cao, *Environ Sci Technol*, 2011, **45**, 4532-4539.

30. S. Zhang, B. Gao and W. Leng, *ACS Appl. Energy Mater.*, 2023, **6**, 1973-1981.
31. X. F. Cheng, W. H. Leng, D. P. Liu, Y. M. Xu, J. Q. Zhang and C. N. Cao, *J. Phys. Chem. C*, 2008, **112**, 8725-8734.
32. P. Pu, H. Cachet, N. Laidani and E. M. M. Sutter, *J. Phys. Chem. C*, 2012, **116**, 22139-22148.
33. B. Klahr and T. Hamann, *J. Phys. Chem. C*, 2014, **118**, 10393-10399.
34. P. Salvador, *J. Phys. Chem. C*, 2007, **111**, 17038-17043.
35. P. Salvador, *Prog. Surf. Sci.*, 2011, **86**, 41-58.